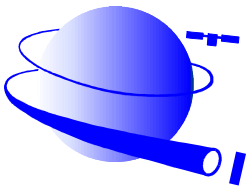

TELECOMMUNICATION
ENGINEERING

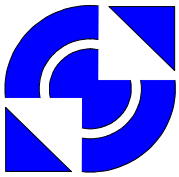

UNIVERSITY
of
TWENTE

University of Twente
Faculty of Electrical Engineering
Chair for Telecommunication Engineering Group

Implementation and tuning of optical single-sideband modulation in ring resonator-based optical beam forming systems for phased-array receive antennas

By Liang Hong

Master thesis
Executed from November 10th 2007 to March 18th 2009
Supervisor: dr.ir. C.G.H. Roeloffzen
Advisors: dr.ir. A. Meijerink
ir. L.Zhuang

Summary

For receiving broadband satellite signal in airplanes, phased array antenna systems can be used instead of conventional satellite dishes, with advantages such as small weight and better aerodynamic performance. The corresponding beam forming and beam steering system can be implemented in the optical domain.

The goal of this master assignment is to analyze and verify the functionality of an optical single sideband filter in the DVB-S receiving system. In order to achieve this goal, the following steps have been taken. First, the frequency response of the filter has been investigated through study its transfer function. The result shows that this filter is not linear in phase, which means that it may introduce signal distortion. Second, the impact of the filter on the modulated signal was studied from the signal pulse point of view. Results are presented for a satellite television case study, based on DVB-S standard. Third, the filter response has been optimized and, and finally the sideband filtering on a double sideband signal has been demonstrate.

The result of the filter analysis indicates that the pulse broadening is quite small and the optimization shows that the filter can be tuned with a value of 25dB suppression and this response can be shifted freely within one free spectra range, without any distortion of the filter response. With this filter response, an optical single sideband suppressed carrier modulation is implemented.

The obtained results show that this optical single sideband filter has a good performance with DVB-S standard signal.

Contents

List of abbreviations and symbols

Abbreviations

AE	antenna element
AR	autoregressive
ARMA	autoregressive moving average
BER	bit error rate
CFGs	chirped fiber grantings
CW	continuous wave
DBSs	direct broadcast satellites
DC	direct current
DSB	double sideband
DTFT	discrete-time Fourier transform
DUT	device under test
DVB-S	digital video broadcasting – satellite
EDFA	Erbium doped fiber amplifier
FIR	finite impulse response
FSR	free spectral range
IIR	infinite impulse response
IMD-2	2^{nd} order intermodulation distortion
ISI	intersymbol interference
ISO	isolator
LO	local oscillator
MA	moving average
MZI	Mach-Zehnder interferometer
MZM	Mach-Zehnder modulator
PDC	predistortion circuit
PM	polarization maintaining
QPSK	quadrature phase shifting keying
RIN	relative intensity noise
RF	radio frequency
SA	spectrum analyzer
SSB	single sideband
SSB-SC	single sideband suppressed carrier
TEC	temperature controller
TTD	true time delay
OBF	optical beam forming
OBFN	optical beam forming network
ORR	optical ring resonator

OSBF	optical single sideband filter

Symbols

α_m	amplitude weighting factor
β	thermo-optic coefficient
γ	losses
$\Delta\phi$	phase of filter response
ϕ_1	phase of the ring
ϕ_2	phase of the MZI
$\Delta\phi_{UL}$	phase difference between upper branch and lower branch of MZI
ψ_s	phase of the signal
γ	bias phase of MZM
τ_g	absolute group delay
τ'_g	normalized group delay
ω	angular frequency
Ω	normalized angular frequency
ν	normalized frequency
v_p	velocity of light in the medium
v_g	group velocity
c_i	through-port transmission
D'	filter dispersion
$E(t)$	electrical field
$E_1(t)$	electrical field upper output directional coupler
$E_2(t)$	electrical field lower output directional coupler
$E_a(t)$	electrical field OBFN output
$E_b(t)$	electrical field OBFN bypass
f_o	optical carrier frequency
f_{RF}	radio frequency carrier
κ	coupling coefficient
κ_{dc}	coupling coefficient of directional coupler
κ_r	coupling coefficient of ring
L_p	smallest optical path length difference of filter
ΔL	length difference between upper and lower path of MZI
p_i	poles
s_i	cross-port transmission

T	pulse duration
T_d	unite delay of the filter
T_m	delay value of the specific antenna element
T_r	delays of the ring
T_t	delay of the MZI
V_π	required modulator bias voltage for π phase difference
V_{ph}	voltage applied on heater

Chapter 1

1 Introduction

1.1 Background

Nowadays the demands of broadband internet and multimedia applications, for example live TV in aircrafts, are growing fast. For this kind of applications, specified communication systems have been designed. They can transmit and receive signals between aircraft and satellites. There are several types of implementation that can be carried out for this purpose. The preferable solution is based on electronic controlled steerable beam phased array antenna systems, since it offers many advantages over mechanical steering antennas such as the reduced weight, fast reaction, and reduces the aerodynamic drag on the aircraft.

A phased-array antenna (PAA) system consists of multiple antenna elements (AEs), and a beamforming network. Implementing the beamforming network in the optical domain instead of electrical domain brings many advantages, such as, compactness, small weight (especially when integrated on a optical chip), frequency independent, immunity to electromagnetic interference, and large bandwidth. An optical beamforming network (OBFN) consists of phase shifters or optical delay elements, and splitting /combing circuitry. An optical ring resonator (ORR) based OBFN has been developed for this system to receive satellite signals. ORR based OBFN can provide continuously tunable true time delay for broadband signals. However, the number of ORRs in the OBFN or namely, the system complexity increases with optical bandwidth requirements [1]. The bandwidth requirement can be minimized by using proper optical signal processing techniques in the system, namely optical single-sideband (SSB) modulation, preferably with suppressed carrier (SSB-SC). In this case, the required OBFN bandwidth is equal to RF bandwidth. There are many different approaches to obtain SSB-SC modulation. In our system, the SSB-SC modulation is achieved by a setup consisting of a Mach-Zehnder modulator (MZM) and optical sideband filter (OSBF). This setup creates a double-sideband suppressed carrier (DSB-SC) optical modulated signal by using MZM, and it suppresses one sideband by

means of the OSBF. One OSBF has been developed for this purpose. The filter is based on ring +MZI structure [2].

1.2 Assignment goal and tasks

The goal of this master assignment is to analyze and verify the functionality of this OSBF in the DVB-S receiving system.

To achieve this goal following aspects have been investigated or demonstrated:

1. Frequency response of filter and its effect on the modulated signal
2. Optimization of the filter response
3. Sideband filtering on a DSB-SC signal

1.3 Report structure

The whole report is based on the tasks listed above. In Chapter 2 the application of the OSBF in the OBFN is explained. In Chapter 3 the analysis of the filter is performed, based on both magnitude response and phase response. In Chapter 4, methods of optimizing the OSBF response are explained, and then the measurement results are presented in Chapter 5. Finally, conclusions and recommendations are written in Chapter 6.

Chapter 2

2 The OSBF in OBFN system

In this chapter, the application of the OSBF in the OBFN is presented.

2.1 System architecture

Our OBFN system consists of a laser, MZMs, OBFN, OSBF, and balanced coherent detector. The schematic of whole OBFN system is shown in Figure 2.1. A setup based on this idea has already been built.

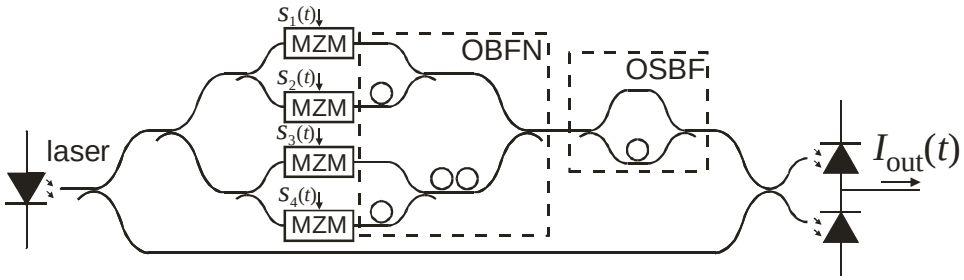

Figure 2.1: Schematic of the novel optical beam forming system

2.2 Overview of optical beam forming system in the receiver system

This optical beam forming system can be used as a component of a satellite receiving system for television and radio broadcasting. We will limit ourselves to the reception of direct broadcast satellites (DBSs), which transmit television signals intended for home reception. using the digital video broadcasting – satellite (DVB-S) standard.

The phased array antenna receives the satellite RF signals from different satellites. The

received RF signal consists of a desired signal in a frequency band 10.7–12.75 GHz. This range is subdivided into many frequency slots of 26MHz to 36MHz with guard bands of 4MHz. Each frequency slot corresponds to a transponder in the system. The typical symbol rates are 22.5 MS/s and 27.5MS/s [3]. The received signal is down-converted to an IF band. This frequency down conversion has been used for two reasons. First, it is required in order to use conventional receivers. Second, the electrical to optical (E/O) conversion costs are reduced as well. After frequency down conversion, an electrical to optical conversion is used to transfer the signals from electrical domain to the optical domain, and then the OBFN synchronizes and combines the signals. Before the desired signal reaches the receiver, an optical to electrical (O/E) converter is used to bring back the signal to the RF domain. So the entire receiving chain is shown in Figure 2.2.

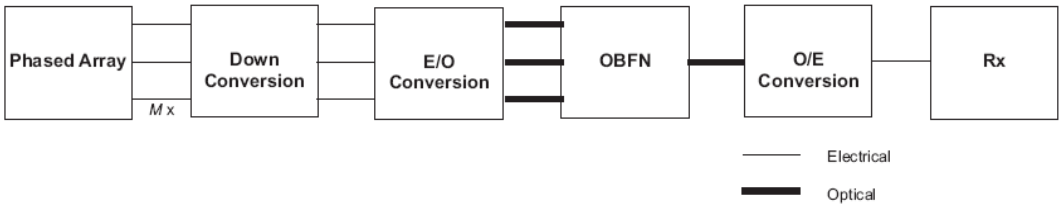

Figure 2.2: Block diagram of optical beam forming system

2.3 Brief description of ORR-based optical beamforming networks

With the resonantly enhanced characteristics, optical ring resonators are able to generate a tunable group delay. By combining multi-stage ORR sections and optical splitters / combiners, the OBFN is achieved. The ORR based OBFN is shown in Figure 2.3

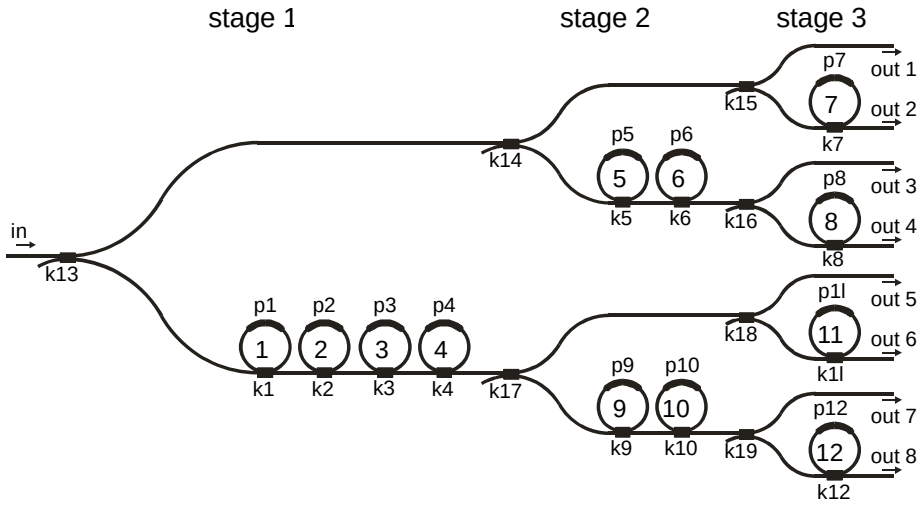

Figure 2.3: Schematic of the binary-tree optical beam forming network

The true-time-delays (TTDs) in the OBFN has a trade-off between peak delay, optical bandwidth relative delay ripple, and number of ORRs, so with large delay tuning range and optical bandwidth requirements, the number of ORRs is increased [1].

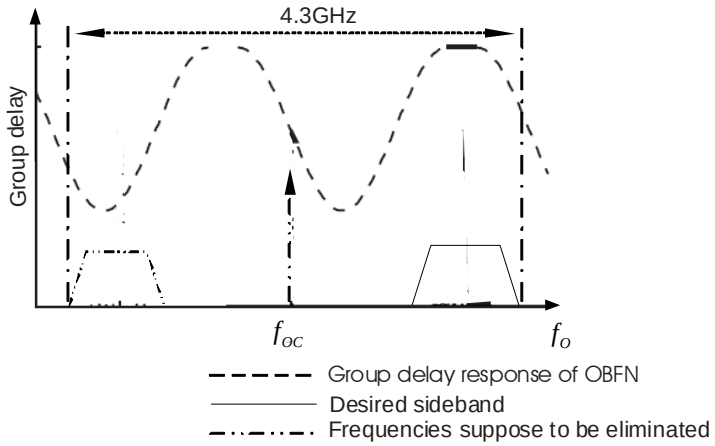

Figure 2.4: The group delay response of the OBFN

As shown in Figure 2.4, the entire optical spectrum takes about 4.3GHz bandwidth. The whole spectrum can be properly synchronized by the OBFN; however, that required a large number of ORR and increases the complexity of the OBFN. Therefore, it is more efficient to synchronize only one sideband of the optical signal by using a proper modulation scheme. Since the two sidebands are identical, there is no information lost when one sideband is suppressed, so single sideband suppressed carrier (SSB-SC) modulation is used for minimizing the optical bandwidth.

2.4 Implementation of SSB-SC modulation

The main reason for using optical SSB-SC modulation here is to reduce the bandwidth of the modulated optical signal, and consequently reduce the complexity of the OBFN. A SSB-SC modulated signal has the same bandwidth as the RF signal. Apart from that, one advantage with respect to optical DSB-SC signal is that the optical detection of SSB-SC modulated signals results in only one beating product at the desired RF frequency, where as DSB-SC modulated signals give two beating products at the desired RF frequency. Those are generally not in phase in case of chromatic dispersion, resulting in RF power fading [1].

Several techniques are known for implementing optical SSB modulation [1]. In this research, SSB-SC modulation is implemented by filter-based techniques, using a MZM to generate DSB-SC and an optical filter, to filter out optically one sideband and the

remaining part of optical carrier. The block diagram of this implementation is shown in Figure 2.5.

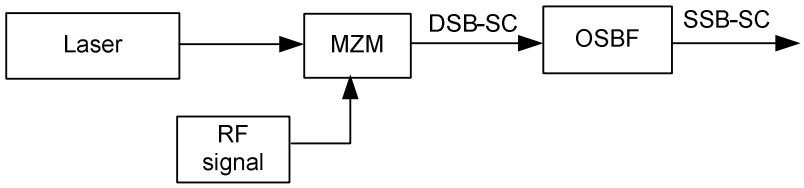

Figure 2.5: Block diagram for implementing SSB-SC modulation

Figure 2.6 (a) is a schematic overview of a dual electrode MZM. The working principle of the MZM is based on the difference in optical path lengths between the upper and lower branch. The electrical fields applied to the branches as a result of the applied voltages are in the opposite directions, the modulator is said to operate in “push-pull” mode. The applied voltage consists of a bias voltage and a modulating signal. Since this MZM modulator is a non-linear device, its output consists of many terms including higher order ones. In order to suppress the even terms of the outcome of MZM, MZM should be biased to correct the value[4].

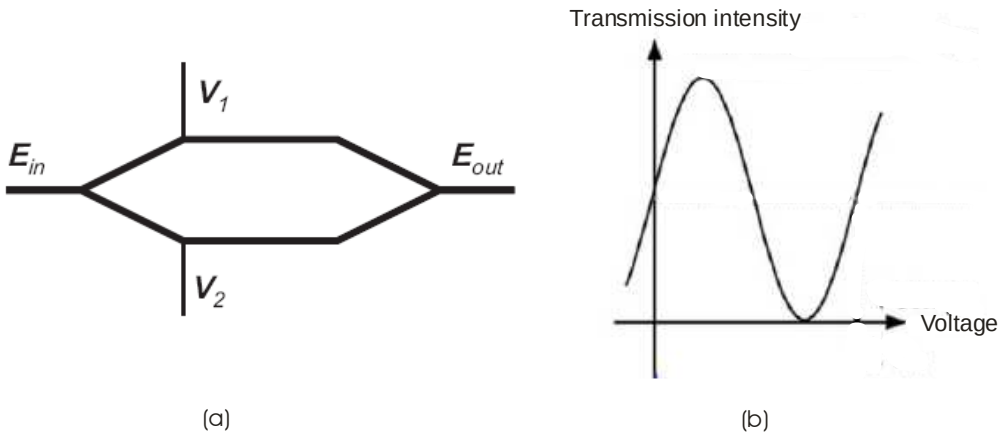

Figure 2.6: Dual electrode MZM(a), The transmission response of MZM (b)

The output signal of MZM is given by [5]:

$$E_{out}(t)=\frac{E_{in}(t)}{2}\{\exp[\mathrm{j}\pi V_1(t)+\mathrm{j}\gamma_1]+\exp[\mathrm{j}\pi V_2(t)+\mathrm{j}\gamma_2]\} \tag{2.1}$$

where γ_1 and γ_2 are the bias phase of MZM. V_1 and V_2 are normalized with respect to V_π. When the MZM is working in the push-pull state, the output is written as [6]:

$$E_{out}(t)=\mathrm{j}\cdot\sqrt{P_o}\cdot\sin(s(t))\cdot\exp(\mathrm{j}\cdot\omega_o t) \tag{2.2}$$

where $s(t)$ is the RF signal, ω_o is the optical carrier frequency, P_o is the input optical power, which can be omitted since it is not interesting in this research. When $s(t)$ is relatively small, then $\sin(s(t)) \approx s(t)$, so the output of MZM can be simplified as:

$$E_{out}(t) \propto \mathrm{j} \cdot s(t) \cdot \exp(\mathrm{j} \cdot \omega_o t) \tag{2.3}$$

The output amplitude spectrum is plotted in Figure 2.7, as can be seen that it is a DSB-SC modulated signal. The amplitudes of the DSB-SC signal scale linearly with the amplitude of the modulation signal, since this amplitude is relatively small. There are several higher order terms in this odd term. However, the first order sidebands are supposed to be larger than the higher order terms.

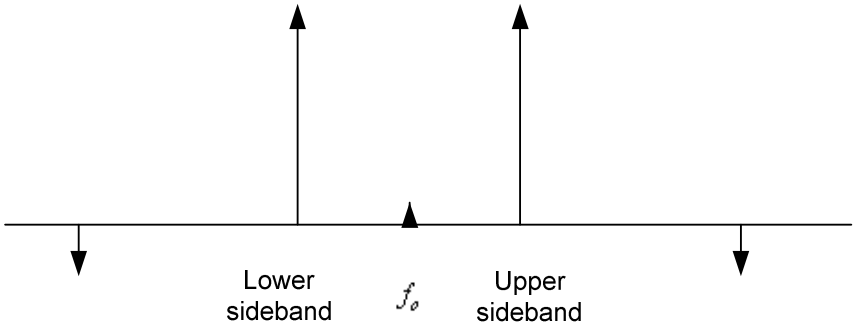

Figure 2.7: Output amplitude spectrum of DSB-SC signal.

In order to generate the SSB-SC signal, one of the sideband from DSB-SC should be filtered out by OSBF, either upper sideband or lower sideband. Figure 2.8 show a case that upper sideband and the remaining part of carrier have been filtered out.

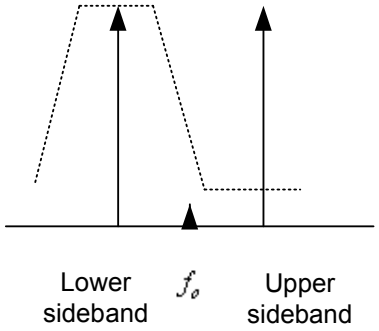

Figure 2.8: Amplitude spectrum of DSB-SC signal with filter curve (dashed)

In principle, the OSBF should be put right after each MZM. However, since the linearity of the OBFN, their order in the system can be reversed, which means that only one common OSBF is required for this system. It has been put at the output port of OBFN, as shown in Figure 2.1.

The optical coherent detection is used to demodulate the optical signal to the electrical domain. It is achieved by combining SSB-SC signal and an unmodulated carrier by a directional coupler before optical detection. The coherent detection configuration with balanced detector is shown in Figure 2.9.

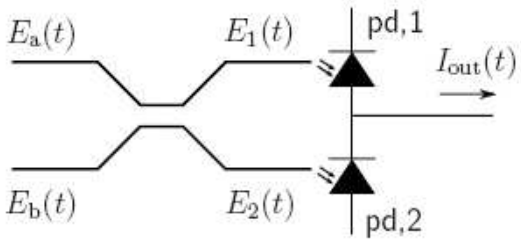

Figure 2.9: Coherent detection with balanced detector

Here, $E_a(t)$ is the filtered signal, and $E_b(t)$ is the bypassed laser carrier. The output of this balanced detector can be written as [4]:

$$I_{out}(t) \propto \mathrm{Im}\{E_a(t) \cdot E^*_b(t)\} \tag{2.4}$$

Chapter 3

3 Optical sideband filter analysis

In this chapter, an MZI+ring filter is analyzed based on digital filter concepts, because the optical filter and the digital filter can be described mathematically in the same way. Therefore, the algorithms developed for digital filters can be used in optical filter analysis as well [7]. First, some basic concepts of filter analysis are presented, and then the frequency response of MZI+ring filter is explained. The filter response is analyzed with a modulated signal as its input to find out the signal distortion introduced by the filter.

3.1 Filter analysis concepts

In this report, we studied the two basic concepts of digital filter analysis, which are the magnitude response and the phase response of the filter.

3.1.1 Magnitude response and phase response

This filter is designed as a linear time-invariant system (LTI) [2], which behaves linearly with respect to the input signals, which are stationary with time. A linear time invariant system is characterized in the time domain by its impulse response $h(t)$. Given an input signal $x(t)$, then the output signal is given by:

$$y(t) = x(t) \otimes h(t) = \int x(\tau)h(t-\tau)d\tau \tag{3.1}$$

Equivalently, in the frequency domain, we have

$$Y(\omega) = X(\omega)H(\omega) \tag{3.2}$$

where the expression in Equation 3.2 are Fourier transforms of Equation 3.1. $H(\omega)$ is the frequency response or transfer function of the filter. The magnitude of $H(\omega)$, $|H(\omega)|$, is called the magnitude response.

$$|H(\omega)| = \frac{|Y(\omega)|}{|X(\omega)|} \tag{3.3}$$

The argument of the frequency response is the phase response of the filter.

$$\phi(\omega) = \arg H(\omega) = \arctan\left(\frac{\mathrm{Im}\,H(\omega)}{\mathrm{Re}\,H(\omega)}\right) \tag{3.4}$$

So the transfer function can be written as:

$$H(\omega) = |H(\omega)| \exp[\mathrm{j}\phi(\omega)] \tag{3.5}$$

In the discrete signal processing theory, a discrete signal may be obtained by sampling a continuous time signal. So $h(t)$, $x(t)$ and $y(t)$ have been replaced by $h(nT_d)$, $x(nT_d)$ and $y(nT_d)$, $T_d = 1/f_{FSR}$ is the unit delay of filter [7], n is the sampling number. Angular frequency ω is normalized to Ω with respect to frequency range with in one period of time $\Omega = \omega T_d$, which is usually referred to FSR, so magnitude response and phase response now be written as:

$$H(\Omega) = |H(\Omega)| \exp[\mathrm{j}\phi(\Omega)] \tag{3.6}$$

$$\phi(\Omega) = \arg[H(\Omega)] \tag{3.7}$$

3.1.2 Steady state

The time domain response of a filter can be expressed as the sum of the transient response and the steady state. The steady state response of the filter for the sinusoidal input signal:

$$x(t) = \frac{A}{2} \cdot \left[\exp\left(j(\omega t + \theta)\right) + \exp\left(-j(\omega t + \theta)\right)\right] \tag{3.8}$$

is given by

$$\begin{aligned} y(t) &= x(t) \otimes h(t) \\ &= \frac{A}{2} \cdot |H(\Omega)| \left[\exp\left(\mathrm{j}\left(\omega t + \theta + \phi(\Omega)\right)\right) + \exp\left(-\mathrm{j}\left(\omega t + \theta + \phi(\Omega)\right)\right)\right] \end{aligned} \tag{3.9}$$

where $\phi(\Omega)$ is the phase response of the transfer function, $|H(\Omega)|$ is the magnitude response of the filter, θ is the initial phase, A is the amplitude[8].

3.1.3 Transient response

Transient response is the response of a filter to a change from equilibrium vice versa. The impulse response of a filter $h(t)$ does not give its transient response directly. For this purpose, we use a different testing signal, i.e. the unit step $u(t)$. The transient response of filter can be expressed in the similar way as we used in 3.1.1, i.e.:

$$y(t) = h(t) \otimes u(t) \tag{3.10}$$

The specific transient response analysis for our filter is performed later part in this chapter.

3.1.4 Group Delay and Dispersion

The filter group delay is defined as the negative derivative of the phase of the transfer function with respect to the angular frequency as follows:

$$\tau'_g = -\frac{d\phi(\Omega)}{d\Omega} \tag{3.11}$$

where τ'_g is normalized to the unit delay, $T_d = 1/FSR$. The absolute group delay is given by $\tau_g = T_d \tau'_g$. The delay is the slope of the phase at the frequency where it is being evaluated, same as the definition in electrical theory. Since the group delay is proportional to the negative derivative of the phase, the group delays are additive.

The filter dispersion, in normalized units, is defined by:

$$D_n \triangleq \frac{d\tau'_g}{df'} = 2\pi \frac{d\tau'_g}{d\Omega} \tag{3.12}$$

For optical fibers, dispersion is typically defined as the derivative of the group delay with respect to wavelength and normalized with respect to the fiber length:

$$D = \frac{1}{L}\frac{d\tau_g}{d\lambda} = -\frac{1}{L}\frac{2\pi c}{\lambda^2}\beta'' \tag{3.13}$$

So the unit is ps/nm/km. The filter dispersion in absolute unit is given by:

$$D = -c\left(\frac{T}{\lambda}\right)^2 D_n \tag{3.14}$$

The unit is ps/nm. The ideal bandpass filter should have linear-phase, constant group delay and zero dispersion, so that they do not distort signals in the passband.

3.2 MZI+ring filter response analysis

One OSBF has been designed by [2]. It is implemented by combining an ORR with an asymmetric MZI. This filter is aimed to suppress one sideband of DSB-SC signal and preserve the other sideband, which forms SSB-SC modulated signal. In addition, this filter can be realized with the same technology as the OBFN, which means it can be integrated with OBFN into a single chip. Here, based on the theory in previous part, the MZI+ring filter is studied in the aspect of magnitude response and phase response

3.2.1 The structure of MZI+ring filter

The structure of MZI+ring optical filter is shown in Figure 3.1. T_d is the unit delay of this filter, $T_d = 1/f_{FSR}$. The signal flow model is shown in Figure 3.2.

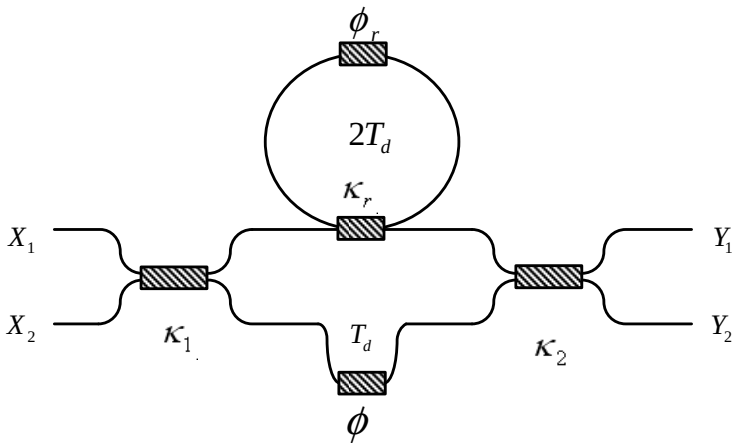

Figure 3.1: MZI+ring filter

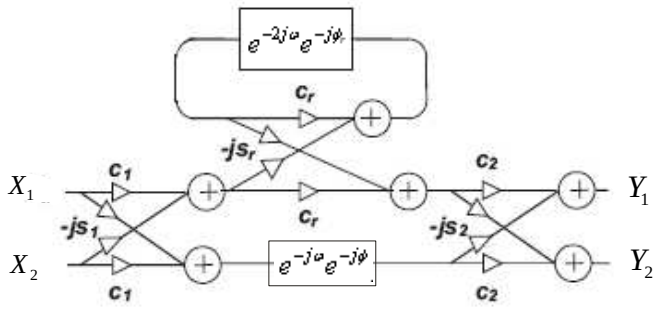

Figure 3.2: Signal flow model of MZI+ring filter

The transfer functions of the filter are given by [2] for $\phi = 0, \phi_r = \pi$ [7]:

$$H_{11}(\Omega) = \frac{c_1 c_2 c_r - s_1 s_2 \exp(-\mathrm{j}\Omega) + c_1 c_2 \exp(-\mathrm{j}2\Omega) - s_1 s_2 c_r \exp(-\mathrm{j}3\Omega)}{1 + c_r \exp(-\mathrm{j}2\Omega)} \tag{3.15}$$

$$H_{12}(\Omega) = -\mathrm{j}\frac{c_1 s_2 c_r + s_1 c_2 \exp(-\mathrm{j}\Omega) + s_2 c_1 \exp(-\mathrm{j}2\Omega) + s_1 c_2 c_r \exp(-\mathrm{j}3\Omega)}{1 + c_r \exp(-\mathrm{j}2\Omega)} \tag{3.16}$$

$$H_{21}(\Omega) = -\mathrm{j}\frac{s_1 c_2 c_r + s_2 c_1 \exp(-\mathrm{j}\Omega) + s_1 c_2 \exp(-\mathrm{j}2\Omega) + s_2 c_1 c_r \exp(-\mathrm{j}3\Omega)}{1 + c_r \exp(-\mathrm{j}2\Omega)} \tag{3.17}$$

$$H_{22}(\Omega) = \frac{-s_1 s_2 c_r + c_1 c_2 \exp(-\mathrm{j}\Omega) - s_1 s_2 \exp(-\mathrm{j}2\Omega) + c_1 c_2 c_r \exp(-\mathrm{j}3\Omega)}{1 + c_r \exp(-\mathrm{j}2\Omega)} \tag{3.18}$$

$H_{nm}(\Omega)$ is the transfer function for the input port X_n and output port Y_m. c_k and c_r are the through port transmission coefficients of the directional couplers of the filter and directional coupler of ORR, which are equal to $\sqrt{1-\kappa_k}$ and $\sqrt{1-\kappa_r}$, respectively; $-js_n$ is the cross port transmission, which is equal to $-\mathrm{j}\sqrt{\kappa_k}$; κ_k and κ_r are the power coupling ratios. In the design [2], $\kappa_1 = \kappa_2 = 0.5$ is used to achieve best filter magnitude response.

The transfer functions for the case that MZI has perfect coupling ratios ($\kappa_1 = \kappa_2 = 0.5$) are:

$$H_{11}(\Omega) = H_{22}(\Omega) = \frac{1}{2}\left(\frac{c_r - \exp(-\mathrm{j}\Omega) + \exp(-\mathrm{j}2\Omega) - c_r \exp(-\mathrm{j}3\Omega)}{1 + c_r \exp(-\mathrm{j}2\Omega)}\right) \tag{3.19}$$

$$H_{12}(\Omega) = H_{21}(\Omega) = \frac{-\mathrm{j}}{2}\left(\frac{c_r + \exp(-\mathrm{j}\Omega) + \exp(-\mathrm{j}2\Omega) + c_r \exp(-\mathrm{j}3\Omega)}{1 + c_r \exp(-\mathrm{j}2\Omega)}\right) \tag{3.20}$$

The impulse response of this bandpass filter can be deduced from the signal flow model of the filter, shown in Figure 3.2, by sending the pulse $\delta(t)$ through the filter.

Impulse response is written as:

$$\begin{aligned} h_{22}(t) &= \exp(-\mathrm{j}\pi)(-\mathrm{j}s)(c_r)(-\mathrm{j}s)\delta(t) + \exp[-\mathrm{j}(\pi+\phi)]c^2\delta(t-T_d) \\ &\quad + \sum_{n=0}^{+\infty}(-\mathrm{j}s)(-\mathrm{j}s_r)(c_r)^n \cdot (-\mathrm{j}s_r)(-\mathrm{j}s)\exp[-\mathrm{j}(n\pi+\phi_r)]\delta[t-2(n+1)T_d] \end{aligned} \tag{3.21}$$

$$= s^2 c_r \delta(t) - \exp(-\mathrm{j}\phi)c^2\delta(t-T_d) + s^2 {s_r}^2 \sum_{n=0}^{+\infty}(c_r)^n \exp(-\mathrm{j}\phi_r)\,\delta[t-2(n+1)T_d]$$

$$h_{11}(t) = c^2 c_r \delta(t) - \exp(-\mathrm{j}\phi)s^2\delta(t-T_d) + c^2 {s_r}^2 \sum_{n=0}^{+\infty}(c_r)^n \exp(-\mathrm{j}\phi_r)\,\delta[t-2(n+1)T_d] \tag{3.22}$$

$$h_{21}(t) = c^2 c_r \delta(t) + \exp(-\mathrm{j}\phi) s^2 \delta(t - T_d) + c^2 s_r{}^2 \sum_{n=0}^{+\infty} (c_r)^n \exp(-\mathrm{j}\phi_r) \delta[t - 2(n+1)T_d] \quad (3.23)$$

$$h_{12}(t) = s^2 c_r \delta(t) + \exp(-\mathrm{j}\phi) c^2 \delta(t - T_d) + s^2 s_r{}^2 \sum_{n=0}^{+\infty} (c_r)^n \exp(-\mathrm{j}\phi_r) \delta[t - 2(n+1)T_d] \quad (3.24)$$

where ϕ and ϕ_r are the extra phase shift of the through arm and the ORR, respectively. We are using $h_{11}(t)$ in the following part of the report for two reasons. First, $h_{11}(t)$ has a stopband bandwidth and a suppression ,which are good enough for generating the SSB-SC signal; second, in the measurement $h_{11}(t)$ can maximize the passband magnitude, while h_{12} has passband suppression. The first term on the right side of equal sign is the part without delay, it goes from X_1 to Y_1 straightly. The second term is the pulse with one unite delay, it comes from X_1 and partially coupled into through arm of MZI, delayed for one unite delay and finally coupled into Y_1. The third term are the pulses, which are coupled into the ring,, delayed for two times unite delay and partially coupled out transfer to Y_1, because of the property of ORR, this term will go to infinite long time.

According to the design, $s = \sqrt{0.5}, c_r = \sqrt{1 - 0.82} \approx 0.4242$ $\phi = 0, \phi_r = \pi$ [2]. Equation 3.22 is simplified as:

$$h(t) = 0.2121\delta(t) - 0.5\delta(t - T_d) + \sum_{n=0}^{+\infty} 0.41 \cdot (-0.4242)^n \cdot \delta[t - 2(n+1)T_d] \quad (3.25)$$

which is plotted in Figure 3.3.

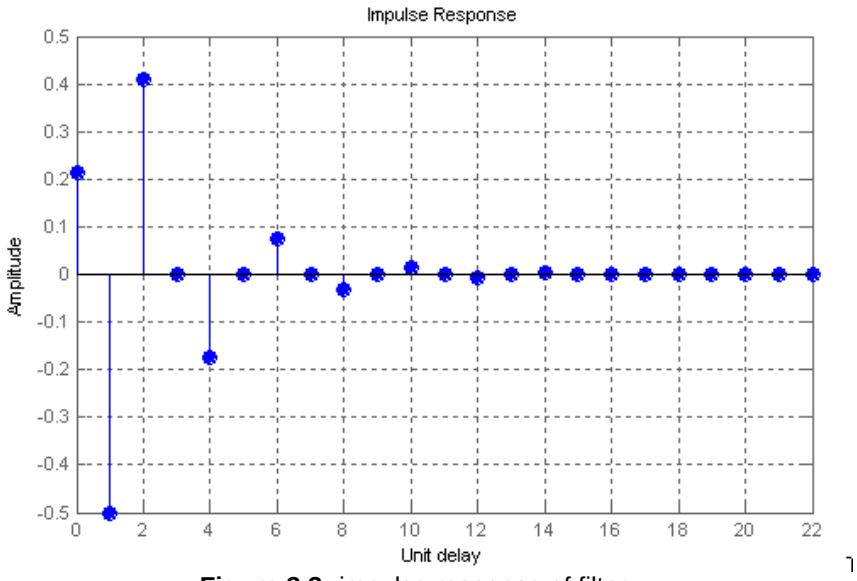

Figure 3.3: impulse response of filter

The even pulses express the property of ring resonator, which is designed to have a delay, which is 2 times larger than the delay of MZI, and goes into infinite time long. All the odd pulse are null except the first one, this pulse is the one from the through arm of MZI, without ring. The amplitude of each pulse is determined by the coupling coefficients of filter.

3.2.2 Analysis of magnitude response

The magnitude response for $\kappa_1 = \kappa_2 = 0.5, \phi = 0, \phi_r = \pi$ is:

$$\begin{aligned} \left|H_{11}(\Omega)\right| &= \frac{1}{2}\frac{\left|c_r - \exp(-\mathrm{j}\Omega) + \exp(-2\mathrm{j}\Omega) - c_r \exp(-3\mathrm{j}\Omega)\right|}{\left|1 + c_r \exp(-2\mathrm{j}\Omega)\right|} \\ &= \frac{1}{2}\frac{\sqrt{(c_r - \cos\Omega + \cos 2\Omega - c_r \cos 3\Omega)^2 + (\sin\Omega - \sin 2\Omega + c_r \sin 3\Omega)^2}}{\sqrt{(1 + c_r \cos 2\Omega)^2 + (\sin 2\Omega)^2}} \end{aligned} \quad (3.26)$$

$$\begin{aligned} \left|H_{12}(\Omega)\right| &= \frac{1}{2}\frac{\left|-\mathrm{j}\left[c_r + \exp(-\mathrm{j}\Omega) + \exp(-2\mathrm{j}\Omega) + c_r \exp(-3\mathrm{j}\Omega)\right]\right|}{\left|1 + c_r \exp(-2\mathrm{j}\Omega)\right|} \\ &= \frac{1}{2}\frac{\sqrt{(\sin\Omega + \sin 2\Omega + c_r \sin 3\Omega)^2 + (c_r + \cos\Omega + \cos 2\Omega + c_r \cos 3\Omega)^2}}{\sqrt{(1 + c_r \cos 2\Omega)^2 + (\sin 2\Omega)^2}} \end{aligned} \quad (3.27)$$

when $c_r = 0.4242$ ($\kappa_r = 0.82$) the magnitude response in dB scale is plotted in Figure 3.4. The solid line is the response of $H_{11}(\Omega)$ when $\kappa = 0.5, \kappa_r = 0.82$, the dotted line is the response of $H_{12}(\Omega)$ for the same parameter.

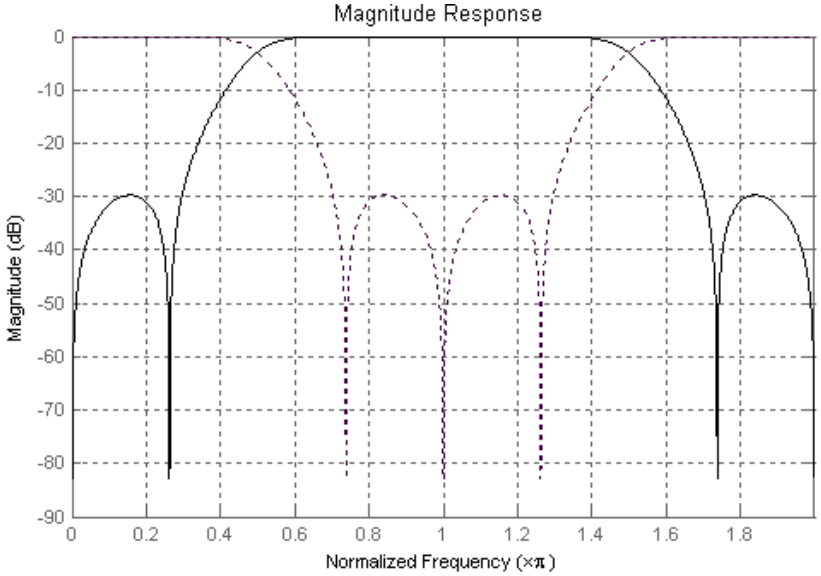

Figure 3.4 : Magnitude response of filter

The responses for different parameters are also shown for comparison. There are more specified analyses about this magnitude response in [2].

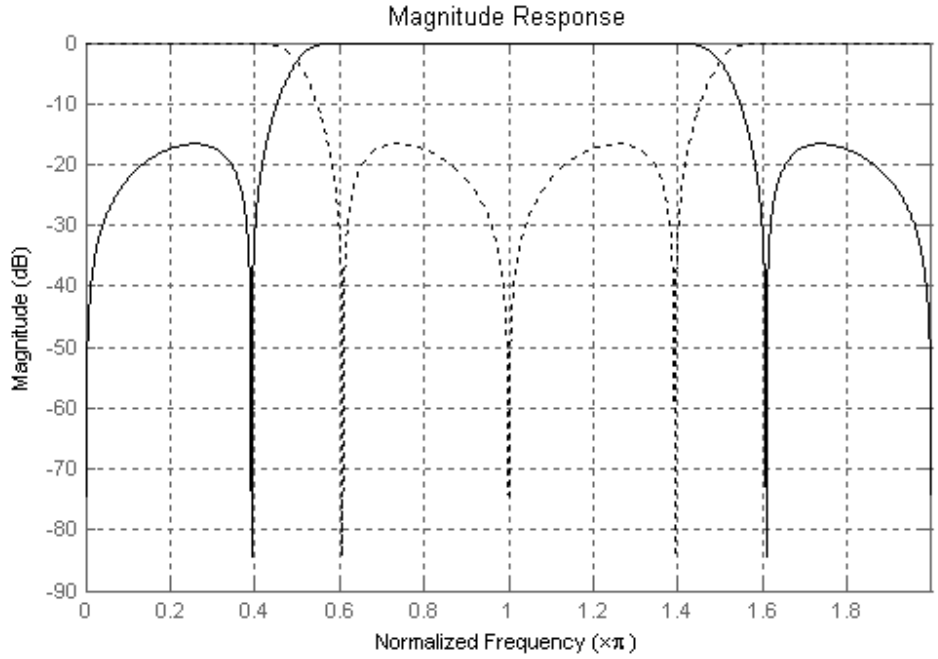

Figure 3.5: Magnitude response of filter

In Figure 3.5, the solid line is the response of $H_{11}(\Omega)$ when $\kappa = 0.5, \kappa_r = 0.7$, the dotted line is the response of $H_{12}(\Omega)$ when $\kappa = 0.5, \kappa_r = 0.7$. For those values the stopband is narrow and suppression is low.

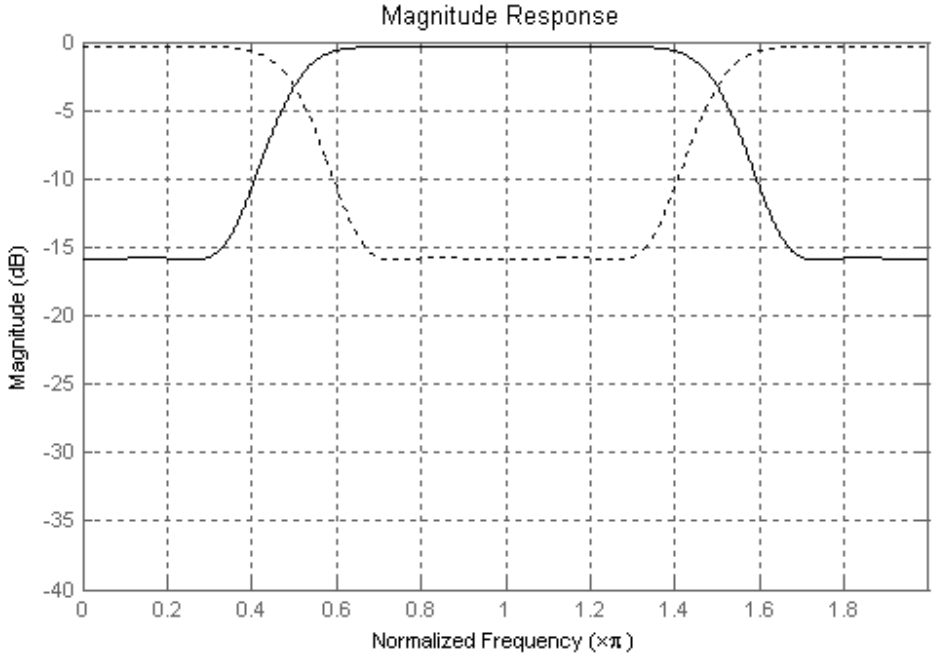

Figure 3.6: Magnitude response of filter

In the Figure 3.6, the solid line is the response of $H_{11}(\Omega)$ when $\kappa_1 = 0.56, \kappa_2 = 0.4, \kappa_r = 0.82$, the dotted line is the response of $H_{12}(\Omega)$ when $\kappa_1 = 0.56, \kappa_2 = 0.4, \kappa_r = 0.82$. In this case, suppression in the stopband is small and there are signal power losses in the passband.

3.2.3 Analysis of phase response

The Phase response is given by:

$$\begin{aligned}\Phi(\Omega) &= \arctan\left(c_r - \exp(-j\Omega) + \exp(-2j\Omega) - c_r \exp(-3j\Omega)\right) - \arctan\left(1 + c_r \exp(-2j\Omega)\right) \\ &= \arctan\left(\frac{\sin\Omega - \sin 2\Omega + c_r \sin 3\Omega}{c_r - \cos\Omega + \cos 2\Omega - c_r \cos 3\Omega}\right) - \arctan\left(\frac{-c_r \sin 2\Omega}{1 + c_r \cos 2\Omega}\right)\end{aligned} \tag{3.28}$$

when $c_r = \sqrt{1 - 0.82}$, the phase response is plotted in figure 3.7.

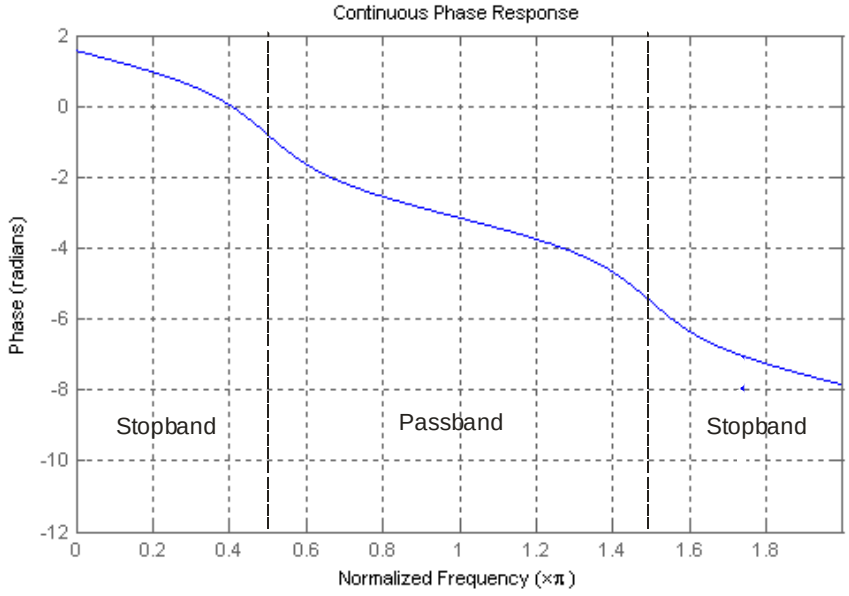

Figure 3.7: Phase response of filter

It is clear that the phase response of passband is not entirely linear in the passband ($0.5\pi \sim 1.5\pi$). The phase non-linearity may cause the signal distortion. Take the derivative of the phase response gives to the group delay response of this filter, shown in Figure 3.8.

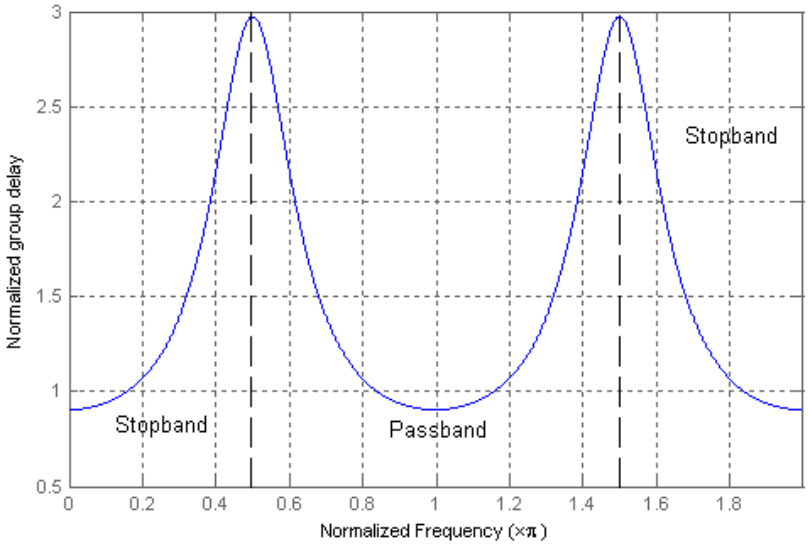

Figure 3.8: Group delay response of filter

As expected, group delay response is not a constant value over the passband, the two peaks are the two frequencies that phase is changing rapidly. The normalized dispersion response is shown in Figure 3.9. It shows the amount of roundtrip per normalized frequency.

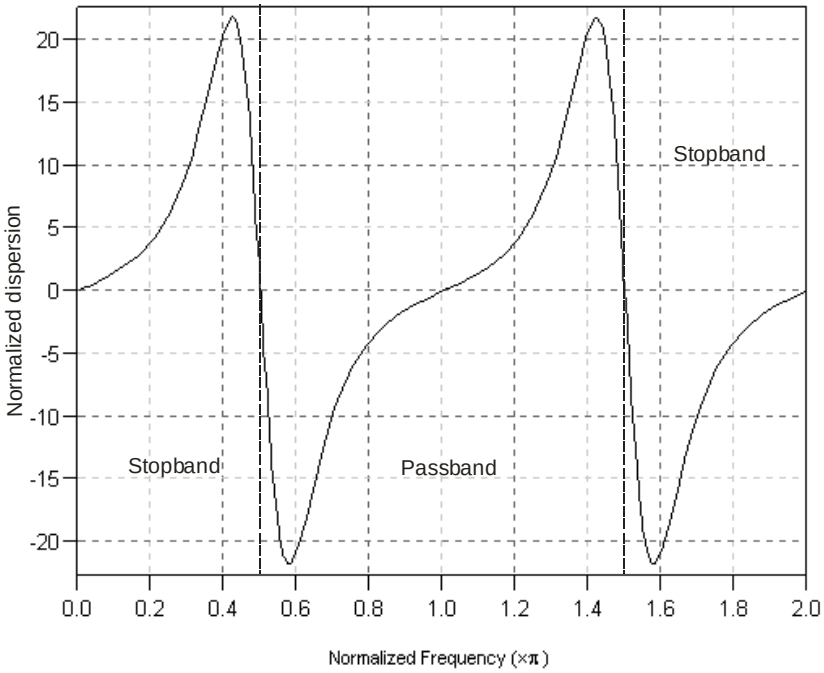

Figure 3.9 : Dispersion response of filter

This dispersion curve shows that the normalized dispersion is zero at the center of the passband and goes from negative to positive in the passband region. From this curve, one can expect that the signal pulses have less pulse broadening when the RF carrier is in the

center of the passband (1.0π) and more pulse broadening when the RF carrier is in the rest part of passband (0.6π). The pulse broadening study is given in the next subsection.

3.2.4 Pulse broadening analysis

From the previous analysis, it is clear to see that normalized dispersion is zero at the center of the passband and goes from negative to positive in the passband region. This dispersion response would bring in signal distortion and pulse broadening for the signals. This signal broadening may produce intersymbol interference (ISI), which may reduce the performance of the receiving system. In order to find out how much the pulse broadening and signal distortion can be introduced by the filter, the signal pulse shape is studied over the entire passband in this part.

The analysis steps are as follows:

1. A digital signal is modulated into RF frequency by means of QPSK modulation [7].
2. This RF signal is modulated into the optical domain, forming a DSB-SC signal by means of MZM.
3. Let this DSB-SC signal pass through the optical filter.
4. The filtered optical signal is demodulated into the RF domain by means of the optical balanced detector.
5. The outcome of the fourth step is demodulated into baseband by means of the QPSK demodulator.

By comparing the demodulated pulse shape with original symbol pulse shape, the pulse broadening and pulse distortion can be seen. The whole procedure is shown in Figure 3.10. All the components are assumed ideal, except the filter.

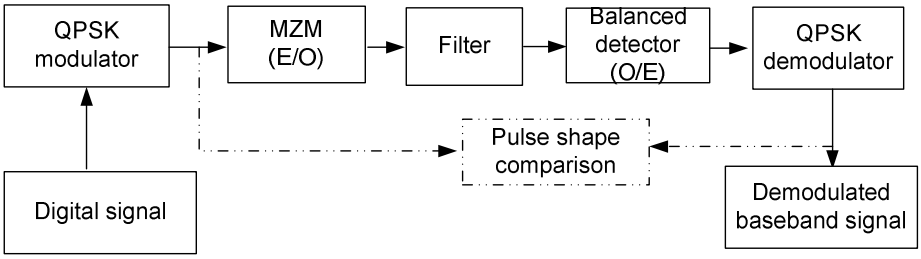

Figure 3.10: Block diagram of pulse distortion analysis

The baseband signal is expressed as:

$$s(t) = \sum_m A_m \cdot p(t - mT_p) \tag{3.29}$$

where $\{A_m\}$ are the data bits that are randomly chosen from the set $A_m \in \{+1, -1\}$. $p(t)$ is the rectangular pulse with a pulse duration of T_p.

This baseband signal is modulated in the "Digital modulator" block by means of QPSK, this modulated signal can be expressed as :

$$s(t) = M_I(t)\cos(\omega_{RF}t) + M_Q(t)\sin(\omega_{RF}t) \tag{3.30}$$

where $M_I(t) = \sum_m A_m p_s\left[t - (2m+1)T\right]$ is called Inphase component of the QPSK signal, $M_Q(t) = \sum_m A_m p_s(t - 2mT)$ is called Quadrature component of the QPSK signal, $p_s(t)$ is the rectangular symbol pulse with a symbol duration of T, it equals to $2T_p$. The carrier frequency is ω_{RF}.

This signal is modulated by MZM to obtain DSB-SC modulated signal. Recall the Equation 2.3 in Chapter 2. The output DSB-SC signal is:

$$\begin{aligned} E_{out}(t) &\propto \mathrm{j}\cdot s(t)\cdot\exp(\mathrm{j}\omega_o t) \\ &= \mathrm{j}\cdot\left[M_I(t)\cos(\omega_{RF}t) + M_Q(t)\sin(\omega_{RF}t)\right]\cdot\exp(\mathrm{j}\omega_o t) \end{aligned} \tag{3.31}$$

ω_o is the optical carrier frequency.

In order to simplify the analysis, the concept of "complex baseband representation" is used here. We use this concept to get rid of the optical frequency in the calculation for both the modulated signal and the filter. In [9], the pre-envelope of the signal $g(t)$ is defined as the complex –valued function:

$$g_+(t) = g(t) + \mathrm{j}\hat{g}(t) \tag{3.32}$$

where $\hat{g}(t)$ is the Hilbert transform of $g(t)$, $g(t)$ is a real-valued narrowband signal. The Fourier transform of the pre-envelope is nothing more than the positive frequency component of the original signal spectrum. That is the reason why a positive sign in the subscript of pre-envelope.

Let the pre-envelope of a narrowband signal $g(t)$ centered about some frequency $\pm\omega$, be expressed in the form

$$g_+(t) = g_z(t)\exp(\mathrm{j}\omega t) \tag{3.33}$$

We refer to $g_z(t)$ as the complex envelope of the signal or the complex baseband representation of the signal. So in this case, the complex envelope $E_z(t)$ of $E_{out}(t)$ is:

$$E_z(t) = \mathrm{j}\cdot\left[M_I(t)\cos(\omega_{RF}t) + M_Q(t)\sin(\omega_{RF}t)\right] \tag{3.34}$$

By using Equation 3.1, the filter output signal $E'_z(t)$ is given by:

$$E'_z(t) = h(t) \otimes E_z(t) \tag{3.35}$$

By combing Equation 3.22 and 3.34, we obtain:

$$\begin{aligned} E'_z(t) = \mathrm{j}\{&s^2 c_r M_I(t)\cdot\cos(\omega_{RF}t) - \exp(-\mathrm{j}\phi)c^2\cdot M_I(t-T_d)\cdot\cos\left[\omega_{RF}(t-T_d)\right] \\ &+ s^2 {s_r}^2\sum_{n=0}^{+\infty}(c_r)^n\exp(-\mathrm{j}\phi_r)M_I\left[t-2(n+1)T_d\right]\cdot\cos\left[\omega_{RF}(t-2(n+1)T_d)\right]\} \\ +\mathrm{j}\{&s^2 c_r M_Q(t)\cdot\sin(\omega_{RF}t) - \exp(-\mathrm{j}\phi)c^2\cdot M_Q(t-T_d)\cdot\sin\left[\omega_{RF}(t-T_d)\right] \\ &+ s^2 {s_r}^2\sum_{n=0}^{+\infty}(c_r)^n\exp(-\mathrm{j}\phi_r)M_Q\left[t-2(n+1)T_d\right]\cdot\sin\left[\omega_{RF}(t-2(n+1)T_d)\right]\} \end{aligned} \tag{3.36}$$

The first curly brackets is the filtered version of inphase component with RF carrier called signal from I channel, $E'_I(t)$; the second curly brackets is the filtered version of quadrature component with RF carrier, called signal from Q channel, $E'_Q(t)$.

This balanced detector is used to demodulate the optical signal as we mentioned in Chapter 2. The expression of the output signal of balanced detector is given by Equation 2.4. In the baseband representation the bypass optical carrier $E_b(t)$ is only a DC, set to one.

The output of this balanced detector i.e., the RF signals can be written as:

$$\begin{aligned} I_{out}(t) &\propto \mathrm{Im}\{E'_z(t)\cdot E^*_b(t)\} \\ &= \{s^2 c_r M_I(t)\cdot\cos(\omega_{RF}t) - \exp(-\mathrm{j}\phi)c^2\cdot M_I(t-T_d)\cdot\cos\left[\omega_{RF}(t-T_d)\right] \\ &\quad + s^2 {s_r}^2\sum_{n=0}^{+\infty}(c_r)^n\exp(-\mathrm{j}\phi_r)M_I\left[t-2(n+1)T_d\right]\cdot\cos\left[\omega_{RF}(t-2(n+1)T_d)\right]\} \\ &\quad +\{s^2 c M_Q(t)\cdot\sin(\omega_{RF}t) - \exp(-\mathrm{j}\phi)c^2 M_Q(t-T)\cdot\sin\left[\omega_{RF}(t-T_d)\right] \\ &\quad + s^2 {s_r}^2\sum_{n=0}^{+\infty}(c_r)^n\exp(-\mathrm{j}\phi_r)M_Q\left[t-(2n+1)T\right]\cdot\sin\left[\omega_{RF}(t-2(n+1)T_d)\right]\} \end{aligned} \tag{3.37}$$

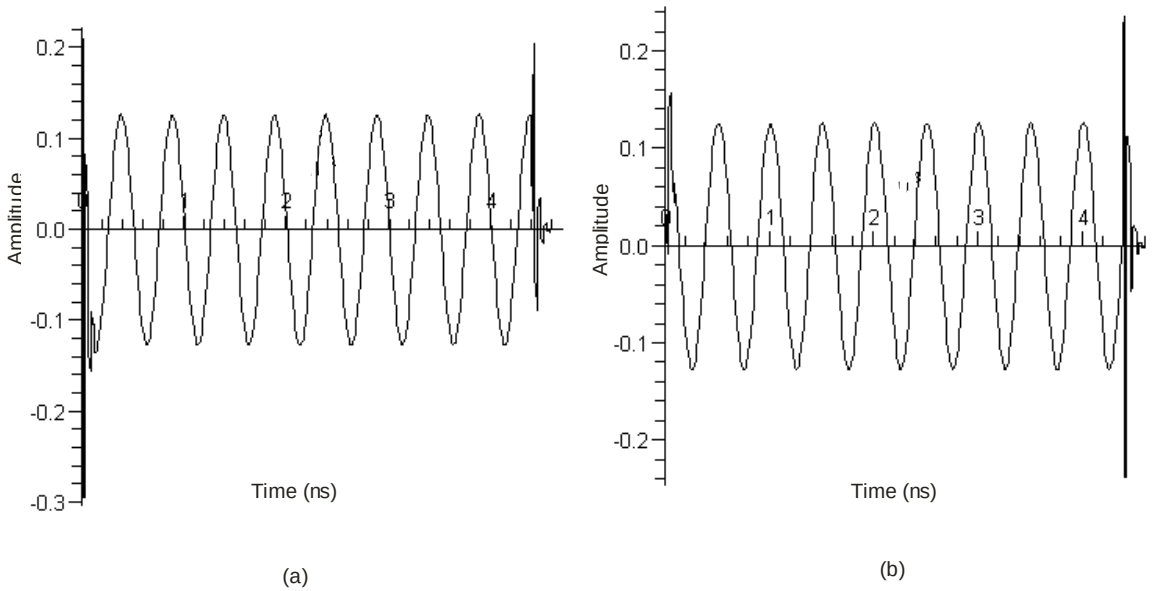

Figure: 3.11: The waveform of I (a), Q (b) component.

Figure 3.11 shows the waveform of I and Q component, corresponding to the first and second curly brackets in the Equation 3.37, respectively. The transient effect of the filter can be seen at the beginning and end of the waveform. It shows that the I and Q components have $\pi/2$ phase offset in carrier. For observing the pulse broadening, we only demodulated one of these two components and its carrier, here we chose inphase component to be demodulated in the inphase channel.

The RF signal is demodulated by a coherent detector, as the block diagram shows in Figure 3.12.

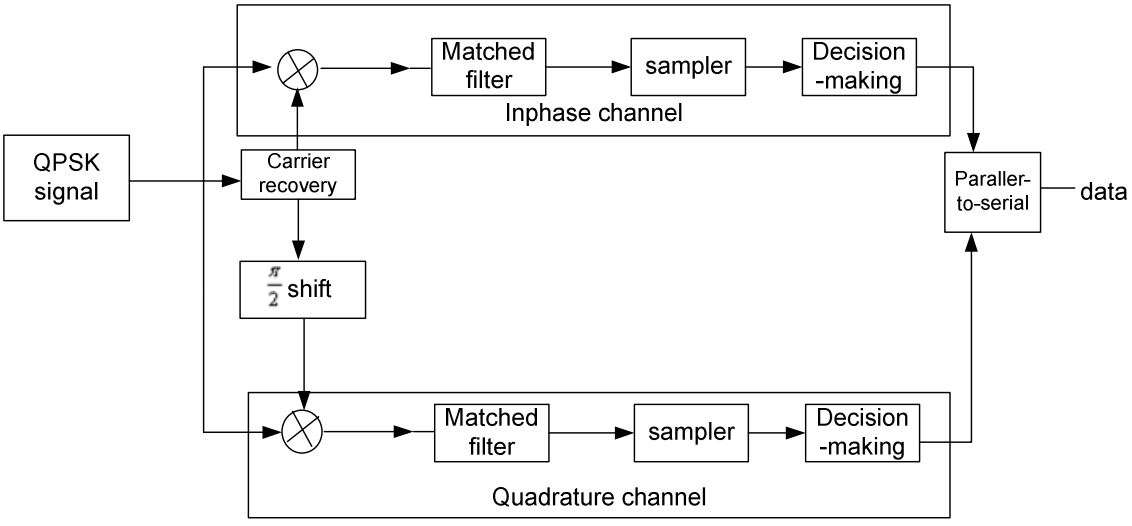

Figure 3.12: Block diagram of QPSK receiver

One can see from Equation 3.37 that there are phase offsets in both I and Q components, because of the unit delay of the filter. The "Carrier recovery" block is able to generate the local oscillator signals, which can lock with both I and Q channel. In this way the QPSK signal can be demodulated with the minimum phase error.

The demodulated QPSK signal is written as:

$$\begin{aligned} s'(t) &= s^2 c_r M_I(t)\cos\left[\phi(\omega)\right] - \exp(-\mathrm{j}\phi)c^2 M_I(t-T_d)\cos\left[\omega_{RF}T_d - \phi(\omega_{RF})\right] \\ &\quad + s^2 {s_r}^2 \sum_{n=0}^{+\infty}(c_r)^n \exp(-\mathrm{j}\phi_r) M_I\left[t-2(n+1)T_d\right]\cos\left[\omega_{RF}\cdot 2(n+1)T_d - \phi(\omega_{RF})\right] \\ &\quad + s^2 c_r M_Q(t)\sin\left[\phi(\omega)\right] - \exp(-\mathrm{j}\phi)c^2 M_Q(t-T_d)\sin\left[\omega_{RF}T_d - \phi(\omega_{RF})\right] \\ &\quad + s^2 {s_r}^2 \sum_{n=0}^{+\infty}(c_r)^n \exp(-\mathrm{j}\phi_r) M_Q\left[t-2(n+1)T_d\right]\sin\left[\omega_{RF}\cdot 2(n+1)T_d - \phi(\omega_{RF})\right] \end{aligned} \tag{3.38}$$

According to the design [2], $s = c = \sqrt{0.5}, c_r = \sqrt{1-0.82} \approx 0.4242, s_r = 0.82$, $\phi = 0, \phi_r = \pi$. Since the data stream is the sum of symbols with the same symbol duration, what happens on one symbol pulse can provide insight of what would happen in the data stream, therefore, we use one symbol in our analysis instead of many symbols. The system is assumed as noise free. The data rate of DVB-S signal is 22.5MS/s and 27.5MS/s.

We know from Section 3.1.2 that the response of filter can be expressed as the sum of a transient response and a steady state. The rectangle pulse is nothing but a sum of two step responses, one rising edge and one trailing edge. Therefore, what happens at the beginning of the pulse and the end of the pulse is more interesting since those are the places where the transient response happened. The remaining parts of the rectangle pulse are just show the state states of the filter, which is flat and have a maximum value of one. Here we only plot the parts where the transient effects happen, it is shown in Figure 3.13. The signal pulses are placed at the center of the passband of this filter.

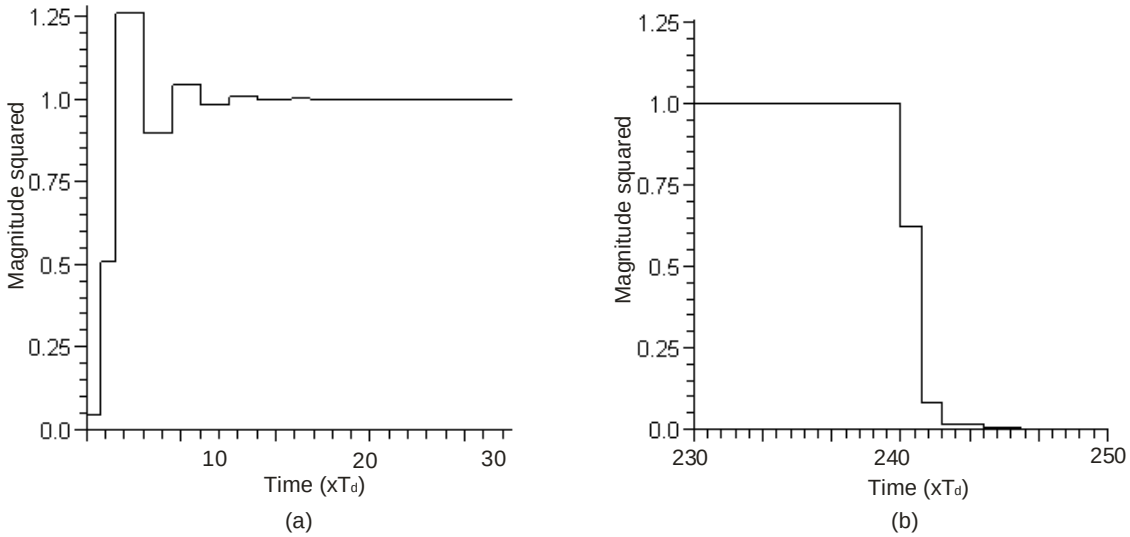

Figure 3.13: The transient response of filter (a) rising stage, (b) trailing edge. The pulse is in the center of the passband.

This output shows that the pulse is broadened compared to the original input symbol time due to the delay property of the filter and the pulse is slightly distorted. It has a stair-like shape; each stair width equals to the filter unit delay $T_d = 1/f_{FSR} = 1/6.7\text{GHz} \approx 0.15\text{ns}$. Those discrete stair-like shapes represent the transient response of the filter. It is determined by the complex coefficients of the filter. There is one stair, which is higher than one; it is due to the discrete time response of the filter that is caused by the unit delay property of the filter. When the RF carrier shifts such as it work in the stopband, the amplitude goes to zero.

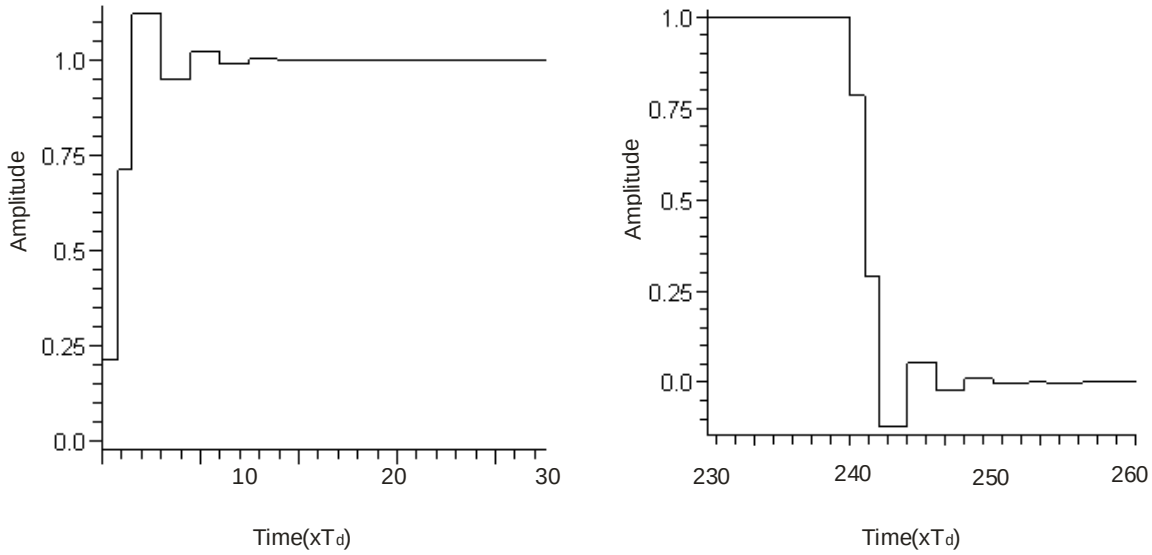

Figure 3.14: The transient response of filter in amplitude (a) rising stage, (b) trailing edge. The pulse is in the center of the passband.

Figure 3.14 shows the transient response of filter in amplitude. The transient responses in the rising stage and trailing edge are symmetric around the center of the pulse. We are not been surprised by this discrete stair-like shape. Since impulse response of the filter is discrete, in the time domain, the convolution result should be discrete as well, though the frequency response is continuous. Since the discrete aperiodic impulse response will have a periodic continuous frequency response. The step response is also deduced from the frequency response [Appendix A].

In the baseband data transmission, eye diagram is used for evaluate the effect of some impairments, for example ISI and receiver noise, on the overall system. Here the eye diagram is also used for evaluate the effect of ISI on this system. The eye diagram is constructed by overlaying plots of the plus shape from successive unit time intervals

Figure 3.15 (a) and figure 3.16 (a) describe the eye diagrams of the output sequence of the filter for the symbol rate of 22.5MS/s and 27.5Ms/s, respectively. As can be seen from these two figures the eye diagram is clean, which indicates a relatively small ISI. Typically, an eye opening of 0.5 or better is considered to yield reliable data transmission [10]. Here the eye opening is much better than 0.5 for both cases, meaning that this filter rarely introduces signal degradation. As described in the beginning of this subsection, the dispersion is larger in the edge of passband than in the center of passband. This means that the pulse is expected to be broadened more when the carrier is in the edge of passband (0.6π) than what it is in the center of passband (1.0π). Figure 3.15(b) and Figure 3.16(b) show the situation when carrier is in the edge of the passband, the pulses are broadened more compared with Figure 3.15(a) and Figure 3.16(a), but not distinct. The magnitude is smaller, that is due to the filtering effect.

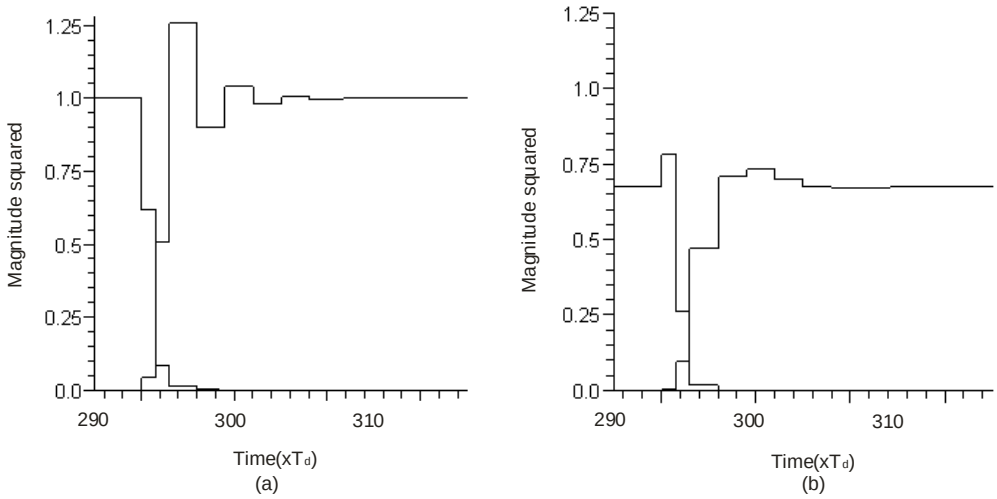

Figure 3.15: The overlapping between two symbols in details. Symbol rate is 22.5MS/s Input pulse at the center of the passband of the filter(a), at the edge of the passband (b).

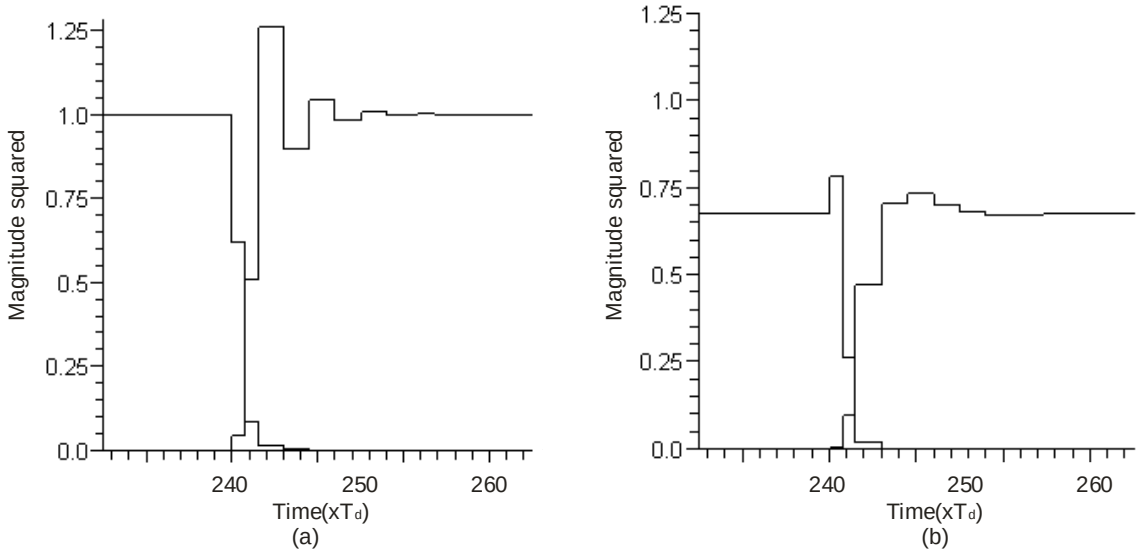

Figure 3.16: The overlapping between two symbols in details. Data rate is 27.5MS/s Input pulse at the center of the passband of the filter (a), at the edge of the passband (b).

From Figure 3.15, one can see that when the symbol duration becomes smaller, i.e., the data rate is larger, the pulse broadening becomes more distinct and the ISI would be larger, because of the unit delay is becoming more obvious compared with the symbol duration. Hence, the signal data rate is considered as a limiting factor of the filter.

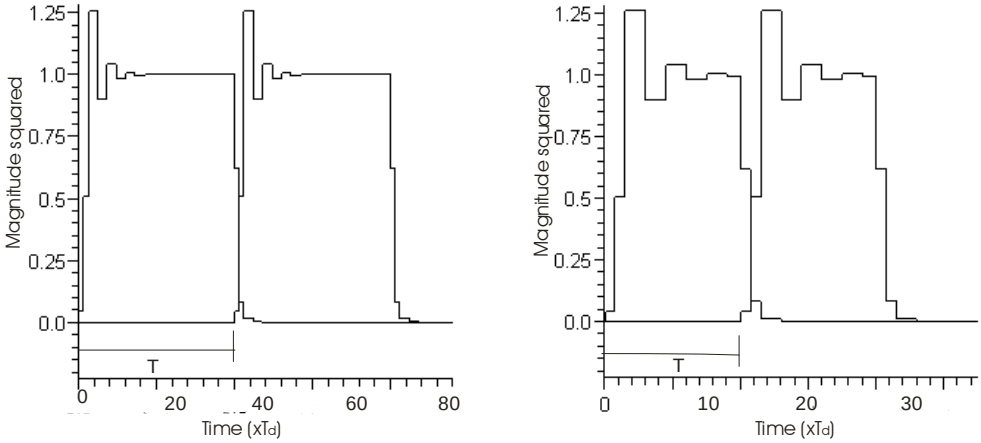

Figure 3.17: Output eye diagram of (a) 200MS/s, (b) 500MS/s

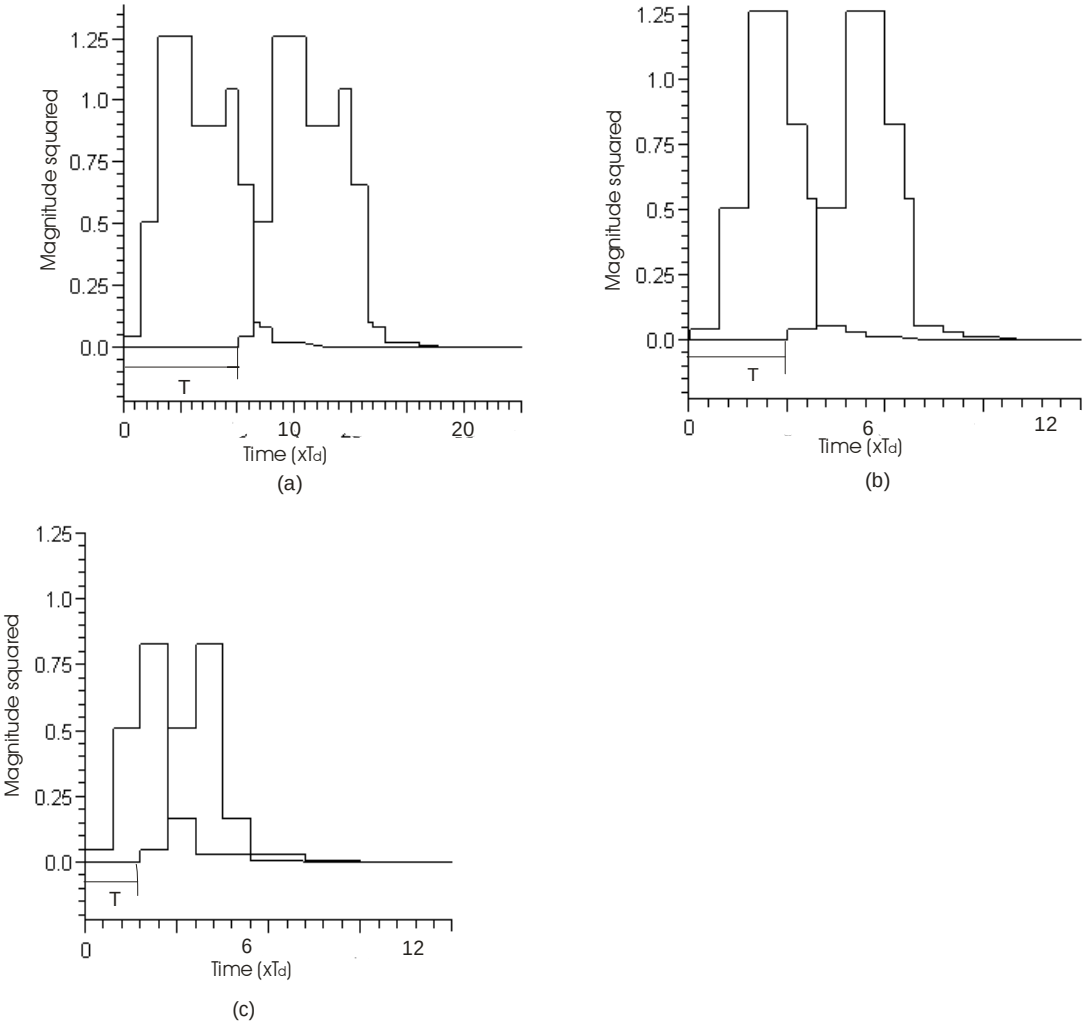

Figure 3.18: Output eye diagram of (a) 1GS/s, (b) 2GS/s, (c) 3Gs/s Input when the carrier is in the middle of the passband.

Figure 3.17 and Figure 3.18 show the eye diagram of the output of the filter with different input data rates. The signal carrier is in the middle of the passband. T is the symbol duration. From Figure 3.17, up to 2GS/s data rate, the eye opening is still good enough to make a sampling without error from ISI. The limiting factor of this filter is the data rate, when the signal carrier is in the middle of passband and the signal is modulated by QPSK modulation scheme, this value is 2GS/s.

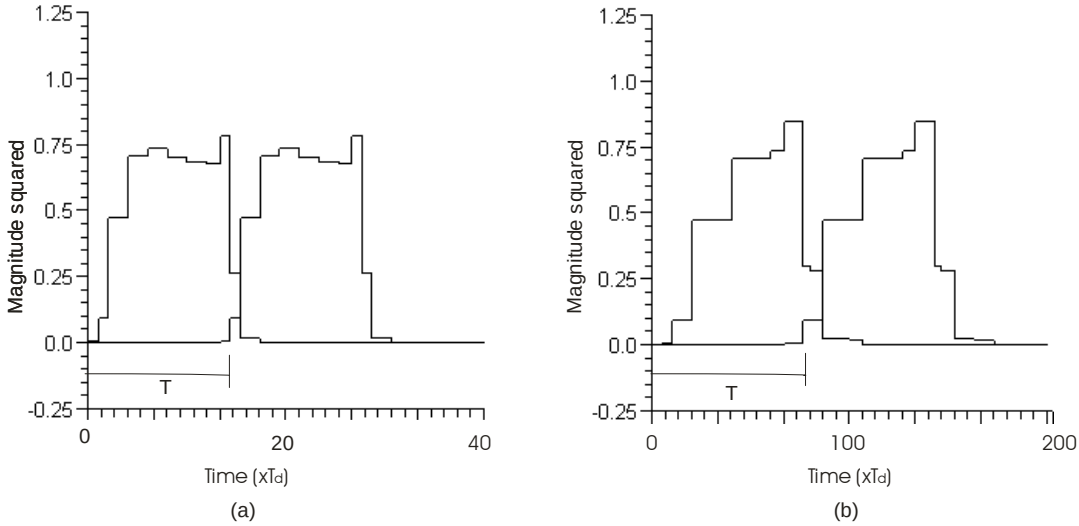

Figure 3.18: Output eye diagram of (a) 500MS/s, (b) 1GS/s when carrier is in the edge of the passband

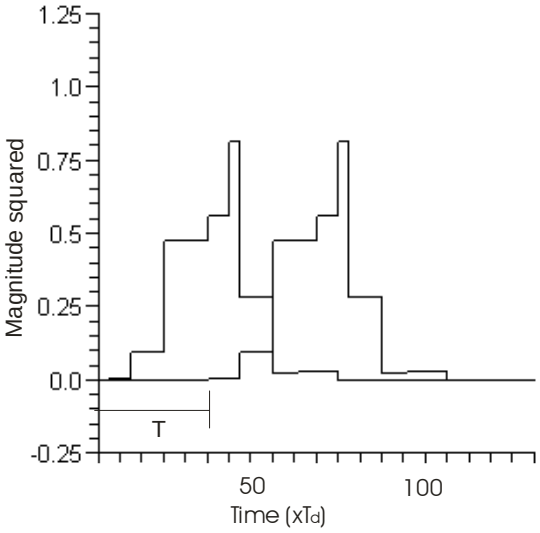

Figure 3.18: Output eye diagram of 2GS/s input when carrier is in the edge of the passband

Figure 3.18 show the eye diagram of the output of the filter with different input data rates. The signal carrier is in the edge of the passband. T is the symbol duration. From Figure 3.18, up to 1GS/s data rate, the eye opening is still good enough to make a sampling without error from ISI. The limiting factor of this filter is the data rate, when the signal carrier is in the edge of passband and the signal is modulated by QPSK modulation scheme, this value is 1GS/s.

Furthermore, the situation when using root raised cosine (RRC) pulse instead of rectangle pulse is shown here.

The expression of a RRC pulse is given by [13]:

$$RRC(t) = \frac{\sin\left(\pi \frac{t}{T_B}(1-\alpha)\right) + 4\alpha \frac{t}{T_B}\cos\left(\pi \frac{t}{T_B}(1+\alpha)\right)}{\pi \frac{t}{T_B}\left(1-\left(4\alpha \frac{t}{T_B}\right)\right)} \tag{3.39}$$

where $T_B = 33ns$ is the inverse of the signal bandwidth, $\alpha = 0.35$ is roll off factor .

The RRC pulse is used to form raised cosine (RC) pulse. The RC pulse provides ISI-free transmission. Normally in the telecommunication system, RRC pulse filters are used both in transmitter as pulse shaping filter and receiver as matched filter. The bandwidth of RRC pulse for DVB-S application is 30 MHz [3]. When the pulse is in the centre and the edge of the passband of filter, the RRC pulse after filter is shown in Figure 3.19.

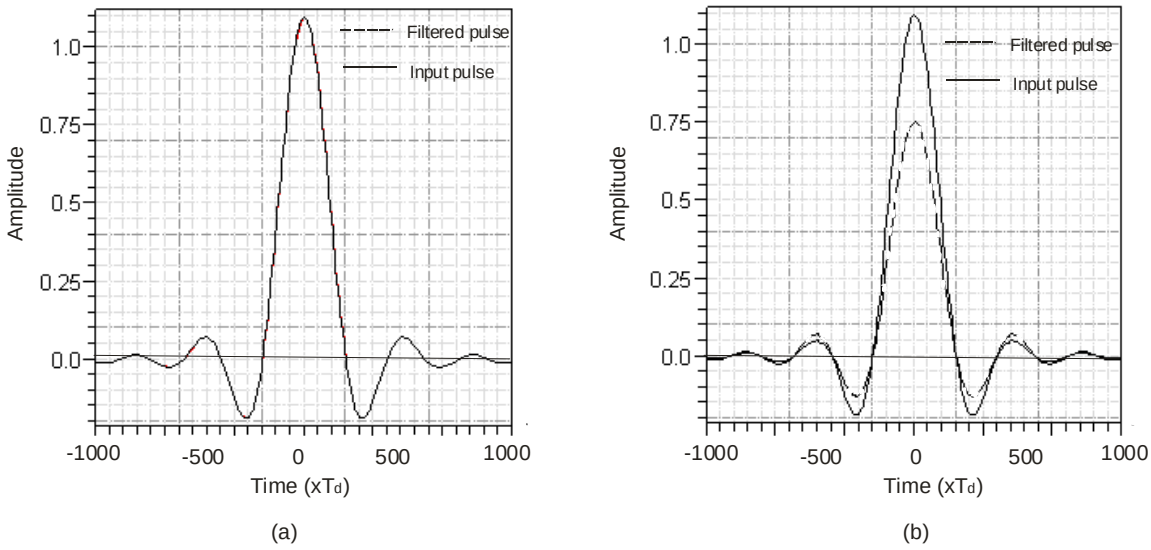

Figure 3.19: The RRC pulse after filtering, (a) in the centre of passband (b) in the edge of Passband.

The solid line is the pulse shape of the input pulse and it is also the shape of matched filter; the dashed line is the pulse shape after filtering. As shown above, the filtered RRC pulse is perfectly fit with the input pulse and the matched filter, when the pulse is in the centre of passband, so an ISI-free RC pulse can be obtained after the matched filter. When the pulse is in the edge of passband,

the amplitude is reduced because of the filtering effect; however, the sampling times do not changed, this means that an ISI-free RC pulse cab be obtained after the matched filter as well.

Chapter 4

4 Practical tuning method

In this chapter, filter-tuning method is explained for the optimization of filter response. This MZI+ring filter is designed as a tunable filter by controlling the different parameters of this filter.

First, the filter response with the related filter parameters are introduced, then the tuning procedure is performed in five steps. The filter can have appropriate response in appropriate wavelength by using this tuning procedure.

4.1 Filter response and filter parameters

This filter is controlled by five parameters. $\kappa_1, \kappa_2, \kappa_3$ are the power coupling coefficients of symmetric MZI coupler(H_1, H_2, H_3), ϕ_1, ϕ_2 are the phase shifters of ring(H_4) and asymmetric MZI(H_5), respectively. Their allocation is shown in Figure 4.1.

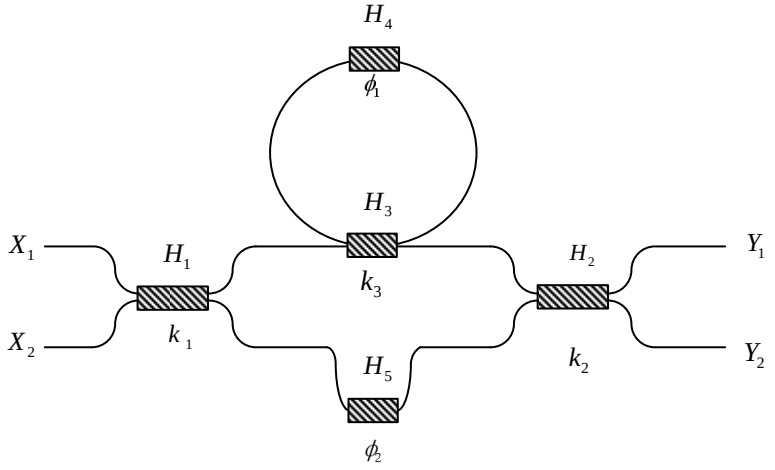

Figure 4.1 Tuning elements on filter

.

The structure of symmetric MZI based tunable coupler is shown in Figure 4.2. A phase shifter is placed into one of two branches to tune the coupler.

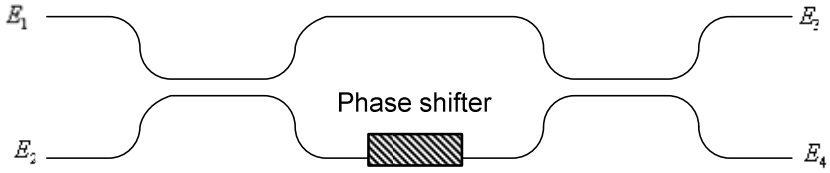

Figure 4.2: Structure of symmetric MZI

E_1 and E_2 are the inputs of the symmetric MZI coupler, in this case only one of these two is used as input; E_3 and E_4 are the outputs of the symmetric MZI coupler. $\kappa_1, \kappa_2, \kappa_3$ can change the phase of the light in one branch by means of phase shifter. This creates the phase difference $\Delta\phi_{UL}$ for certain wavelength of laser between the upper branch and lower branch. Then on the directional coupler the constructive interference or, destructive interference, or some kinds of interferences in between could happen, the output power as a function of $\Delta\phi_{UL}$ is [12]:

$$P_{out} = P_{in} \cos^2 \frac{\Delta\phi_{UL}}{2} \tag{4.1}$$

So the κ_1 determines the amount of laser power going through upper branch and lower branch of the filter. The κ_2 has the same functions as κ_1, it determines the laser power in the output ports (Y_1 or Y_2). The stopband suppression of this MZI+ring filter is determined by κ_1 and κ_2. $\kappa_1 = \kappa_2 = 0.5$. This value makes sure that there is always a zero on the unit circle, no matter which inputs or outputs are used [7].

κ_3 is the coupling coefficient of ORR, it determines the power couple in and out of ORR, hence the pole magnitude c_r ($c_r = \sqrt{1-\kappa_r}$) of the ORR. For an ORR with loss, the antiresonance condition equates to the frequency with maximum transmission of the ORR, while the minimum transmission of the ORR occurs at resonance frequency. As a function of the pole location, the nonlinear phase response is given by [7]:

$$\Phi_r(\Omega) = \arctan\left[\frac{(1-c_r^{\,2})\sin(\Omega T_r + \phi_1)}{2c_r - (1+c_r^{\,2})\cos(\Omega T_r + \phi_1)}\right] \tag{4.2}$$

The phase response for two different κ_r is compared in Figure 4.3 with $\phi_1 = \pi$.

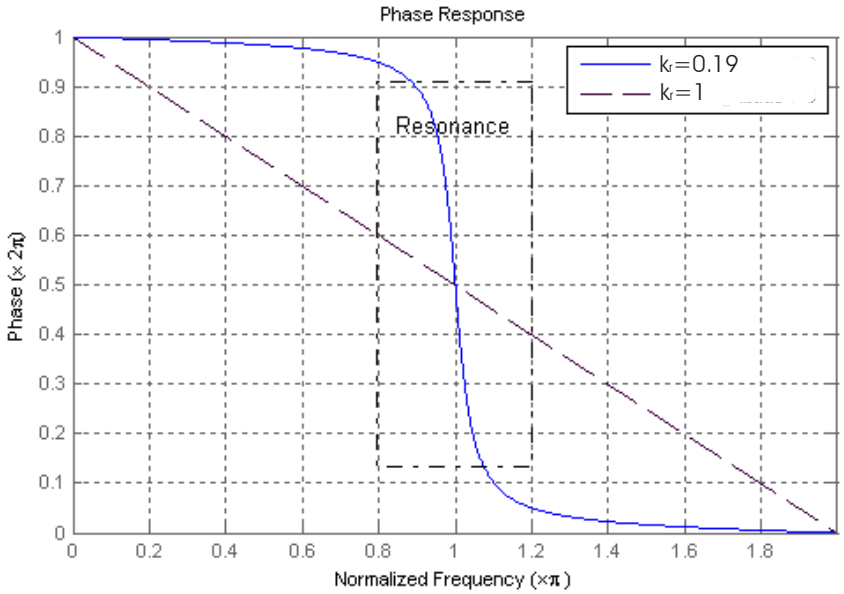

Figure 4.3: Phase response for an ORR with two different pole magnitudes.

For the $c_r = 0.9$ case, the phase of the ORR changes abruptly at resonance frequency, which correspond a narrow stopband bandwidth; Off-resonance frequency, the phase of the ORR changes much more slowly, which correspond to a wide passband bandwidth.

The ϕ_1 is the phase shifter of the ORR, it changes the resonance frequency of ORR, i.e., the phase of ORR. ϕ_2 is the phase shifter of through path of asymmetric MZI, it changes the phase of this path. The passband and stopband center frequencies occur where the phase difference between the ORR and the through path of asymmetric MZI is an integer multiple of π [7]. The phases for each arm of the MZI are illustrated in Figure 4.4, for $\phi_1 = -\pi$, ϕ_2 =0.

The center frequency of the filter can be changed with this phase relations as well. One only needs to change the value of ϕ_1 and ϕ_2 while keep the phase difference of ORR and through arm equals to integer multiply by π.

In order to flatten the passband, a constant phase difference around the passband center frequency is required. It can be achieved when the slop of the ORR's phase response equals to the slop of the through arm phase response at the passband center frequency[7], as it shown in Figure 4.4. This can be done by changing the value of c_r, which changes the

phase response of the ORR in such that there is a rapid changing phase in the resonance frequency, while slowly changing phase at off-resonance, making passband flattened.

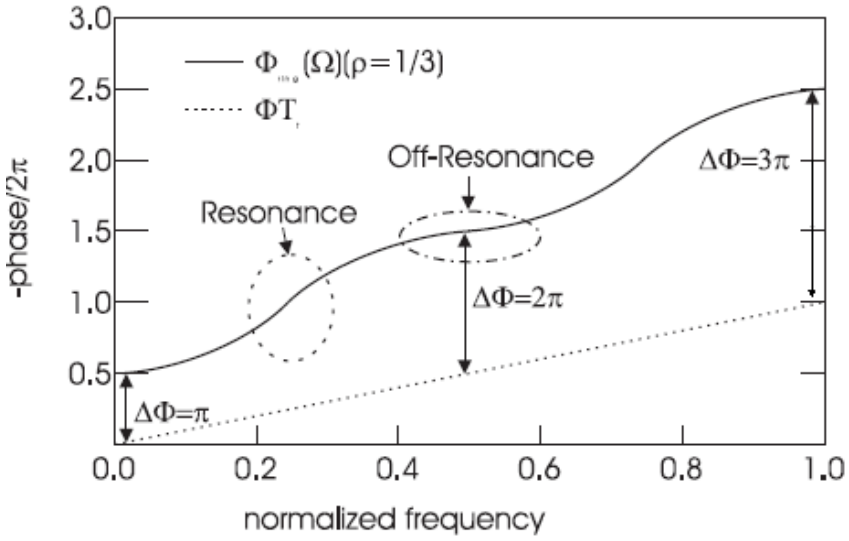

Figure4.4: The phase response for each arm of the MZI

With the appropriate parameters $\kappa_1 = \kappa_2 = 0.5, \kappa_r = 0.82$, $\phi_1 = \pi$, $\phi_2 = 0$ the filter response $\left|H_{11}(\Omega)\right|$ is shown in Figure 4.5.

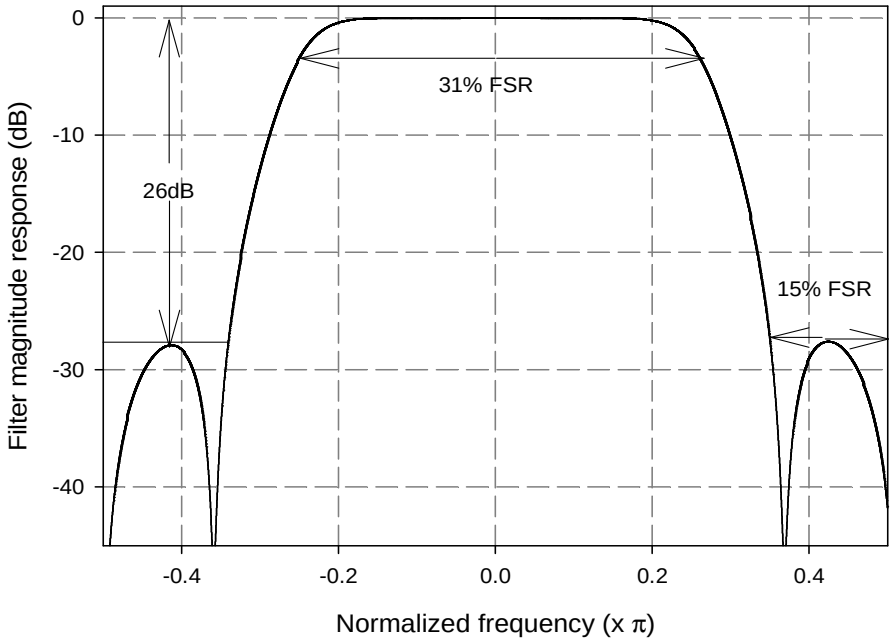

Figure 4.5 Filter Magnitude responses in theory

4.2 Filter tuning procedures

The ideal values of different parameters are described in the previous section. The tuning procedure shows the way of obtaining those values in a real filter. The procedures are given as follow:

Step 1: Set $\kappa_1 = \kappa_2 = 0.5$:

- The optimization started form finding out the best coupling coefficients of two couplers of the asymmetric MZI, 0.5 for both two of them. In order to find out the value of $\kappa_1 = \kappa_2 = 0.5$, we need to find out $\kappa_1 = \kappa_2 = 0$ as reference value, this situation usually referees to the bar state of MZI. The signal flow of the bar state of MZI is shown in Figure 4.6, from X_1 to Y_1. Tune the value of κ_1 and κ_2, the filter response should shift up until the filter response reaches the maximum value, this means $\kappa_1 = \kappa_2 = 0$ as shown in Figure 4.7 dot-dash line. The dips are the response of the ORR, which behave periodically. Then we can reduce the value of κ_2 until this filter magnitude response is 3dB lower than the situation when $\kappa_1 = \kappa_2 = 0$, as it shows in Figure 4.4 solid line. At this moment $\kappa_2 = 0.5$. Repeat it again, but set $\kappa_2 = 1$ then reduce the value of κ_1, the filter magnitude response of ring should be the same as former one. At this moment $\kappa_1 = 0.5$.

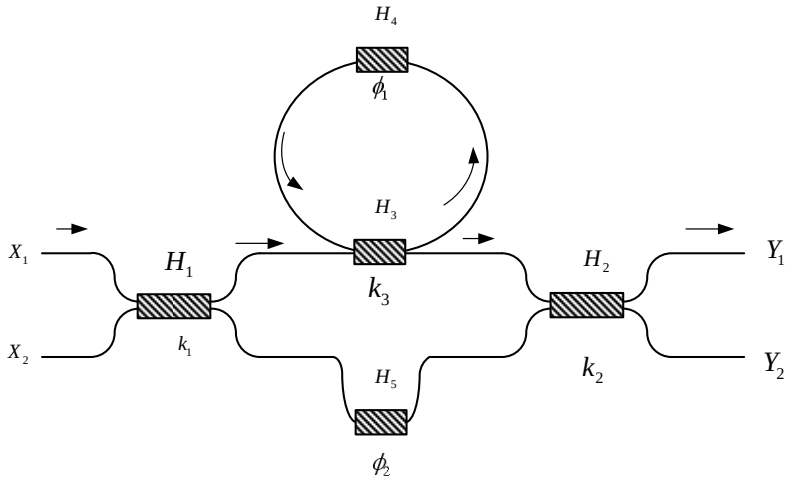

Figure 4.6: Signal flow when the MZI is working in the bar state, from X1 to Y1

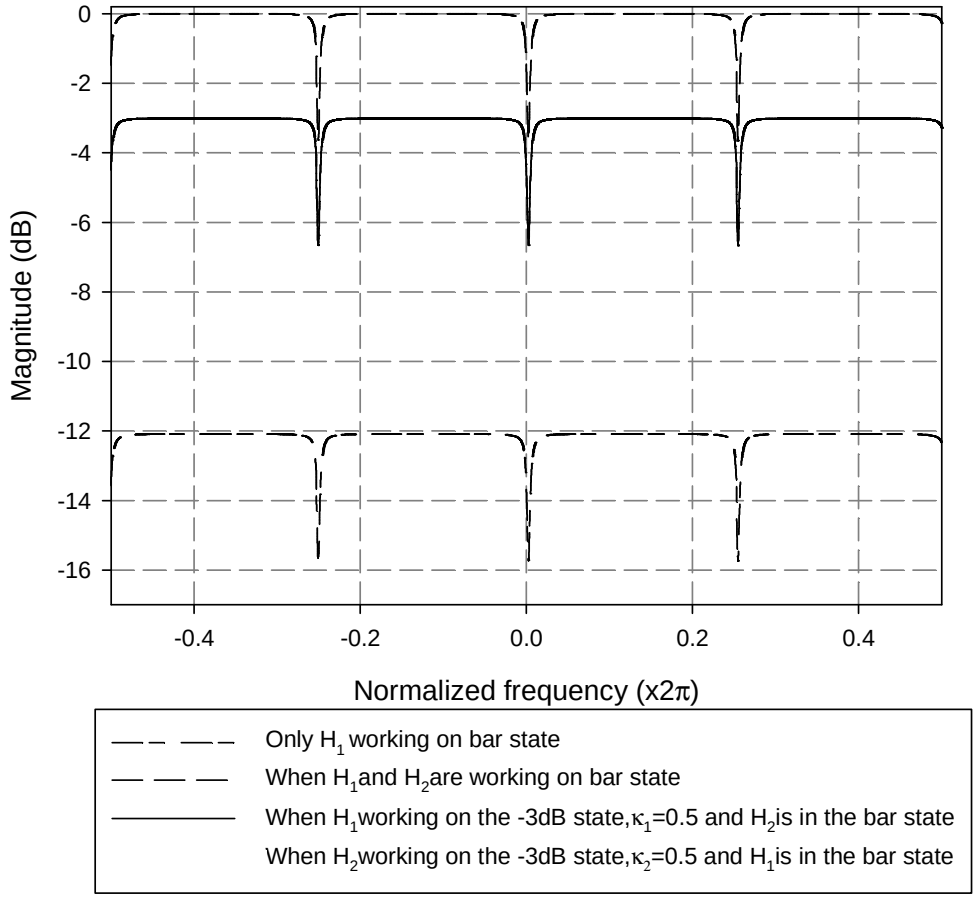

Figure 4.7: Magnitude response when ORR takes part in the filter.

Step 2: Set $\phi_1 = \pi, \phi_2 = 0$

- Set $\kappa_1 = \kappa_2 = 0.5$. Take ϕ_2 as reference value, tune ϕ_1 until the passband and stopband of the filter can be observed. The phase relation shown in Figure 4.4 is achieved The filter response should be bilateral. It is shown in Figure 4.8.

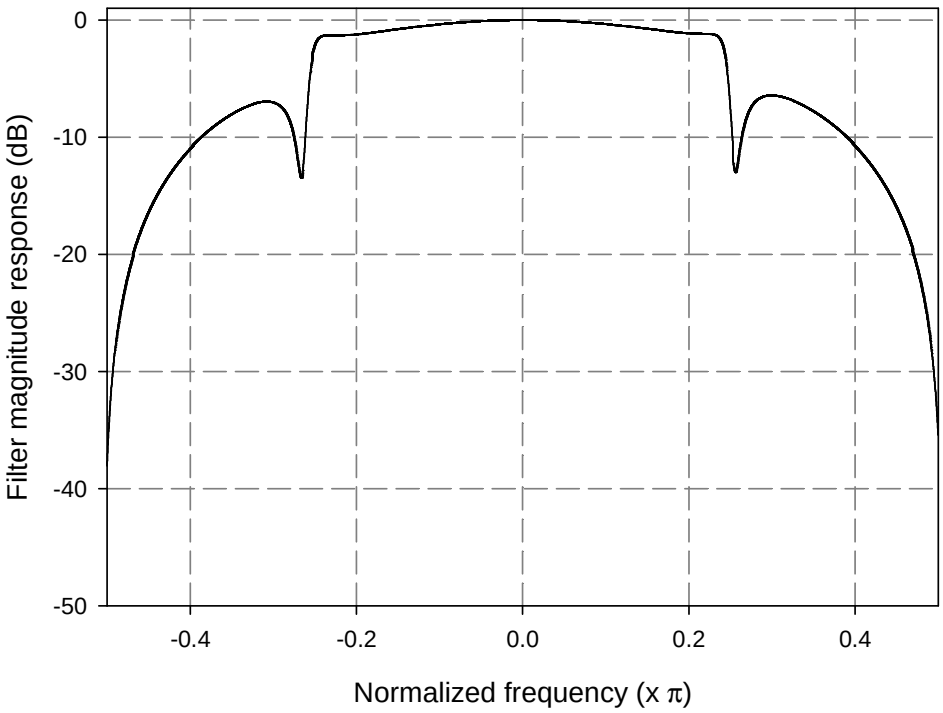

Figure 4.8: Filter response when $\phi_1 = \pi, \phi_2 = 0$

Step 3: Set $\kappa_3 = 0.82$

- Using the parameters from the Step 2 and Step 3, one need to increase or decrease the value of κ_3 until the passband flattening is achieved and the suppression meet the requirement. However, κ_3 controls a MZI based coupler, when κ_3 changes, the phase of the ORR is changed, the phase difference between ORR and the through path is changed as well, so one should tune ϕ_1 at the same time to adjust this variation. The filter response should have at least 25dB suppression; the passband takes 31% of one FSR. Some fine-tunings of each parameter may require in order having the optimized filter response, the result is shown as in Figure 4.5.

Step 4: Shift the filter to the appropriate frequency.

- In theory this filter response can be shift to the appropriate frequency by tuning the phase shifter ϕ_1 and ϕ_2. It should be in such a way that the phase difference between

ORR and the through path should not be changed. ϕ_1 and ϕ_2 should be tuned together, basically $\Delta\phi_1 = 2\Delta\phi_2$. The filter response shifting is show in Figure 4.9. The solid line is the initial position, the dot line, and the dash line show that the filter response is shifting to the right.

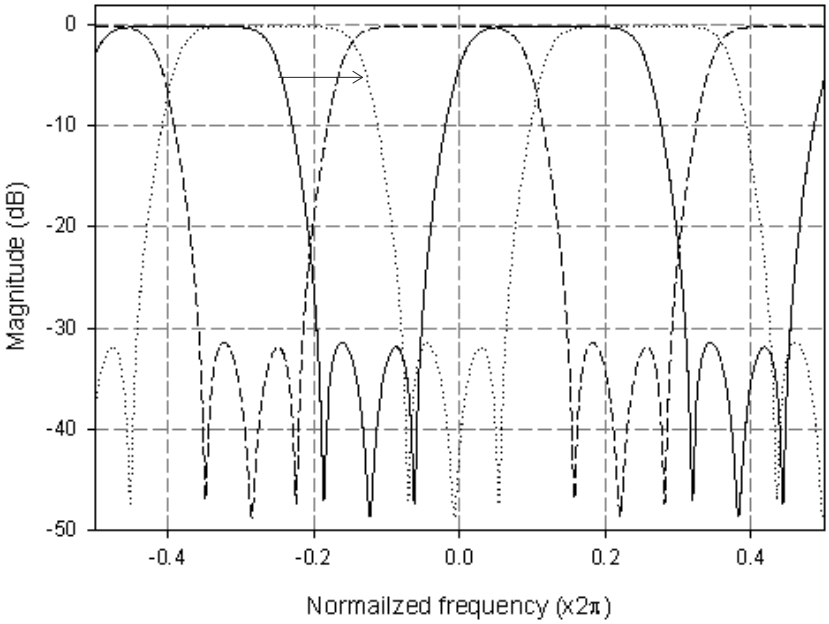

Figure 4.9: Filter response shifting

Chapter 5

5 Measurements

This chapter presents the measurement results of filter response using the tuning method in Chapter 4 and demonstrates the SSB-SC modulation. There are two measurement setups; one for measuring filter magnitude response and phase response, the other one is used for measuring and demonstrating the SSB-SC modulation.

5.1 Filter magnitude response

The measurement setup is shown in Figure 5.1, the solid line is the optical path, and dash line is electrical path. This setup has been used for measuring the magnitude response (this section) and the group delay response (next section) of the filter. The working details are shown as follow: the laser current source is ramping between a smaller and larger current, so that the laser frequency is changing in a certain frequency range in order to create certain optical bandwidth. This ramping signal is also synchronizing the network analyzer. Laser temperature is kept in stable by temperature controller (TEC). The MZM modulator superposes an RF signal on the optical carrier, and goes through the optical chip (DUT). Since the laser power is too low to detect after passing through the optical chip, it is amplified by an EDFA. Then the amplified signal is detected by optical detector. It measures the amplitude and the phase of signal and feed into the second port of network analyzer. The measurement result is plotted in Figure 5.2. It shows the magnitude response of the filter in one FSR. The suppression is around 25dB

The filter is tuned properly with the method in Chapter 4. In this measurement, the filter tuning method is implemented by thermo-optic effect.

The filter magnitude responses measured with the same type of filter but with different fabrication parameter compared with the filter used for group delay response measurement.

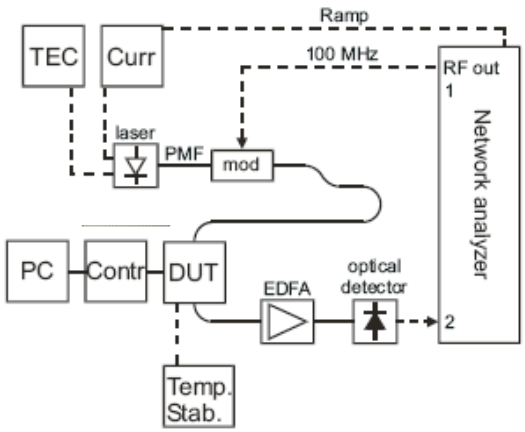

Figure 5.1: Setup for measuring filter transmission response. TEC is temperature controller for the Laser. Curr is current controller for the laser. It generates periodic ramping current. It controlees the Network Analyzer. DUT is device under test, it is the optical chip in this case. Mod is MZM modulator. PC is the computer, Contr is control system. EDFA is erbium doped fiber amplifier.

The measured filter response is shown in Figure 5.2. The result has been nicely fitted with theoretical curve ($\kappa_1 = \kappa_2 = 0.51, \kappa_3 = 0.84$, loss of the ORR 0.5dB/cm). Filter magnitude response has been measured in one FSR, suppression is around 25dB. It shows clear flattened passband and broadened stopband. The passband takes around 20GHz.

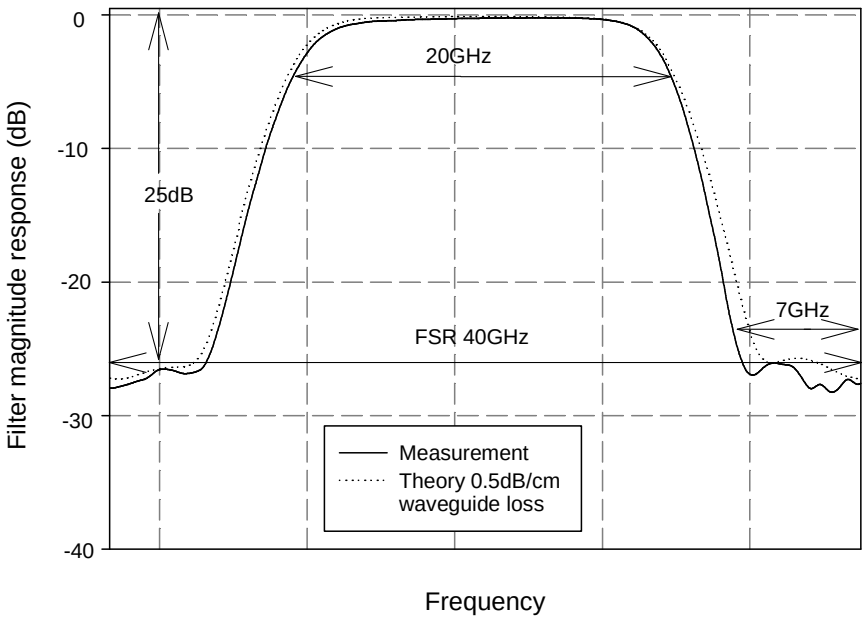

Figure 5.2: Filter optical magnitude response in bar state

The filter response can be shifted by changing the values of phase shifters. In general, the phase shift of ring resonator and MZI as a function of the applied power is [13]:

$$\Delta\phi = a \cdot P \tag{5.1}$$

in which a is coefficient, P is the power applied on heater. The $\Delta\phi$ is the phase shifting range of ORR and MZI. It is a linear function. Figure5.3 shows the phase shift of ORR (solid line) and MZI (dotted line) as function of the power applied on the heater.

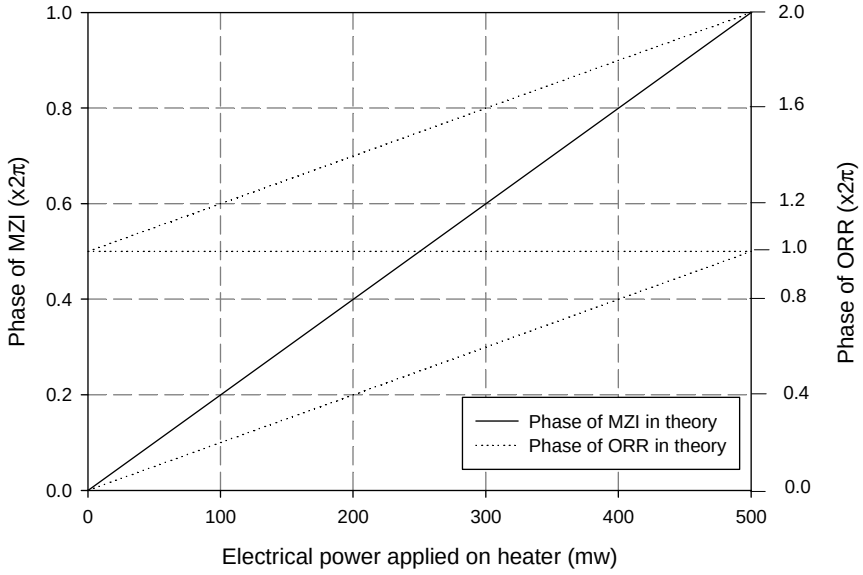

Figure 5.3: Phase and power relation in theory

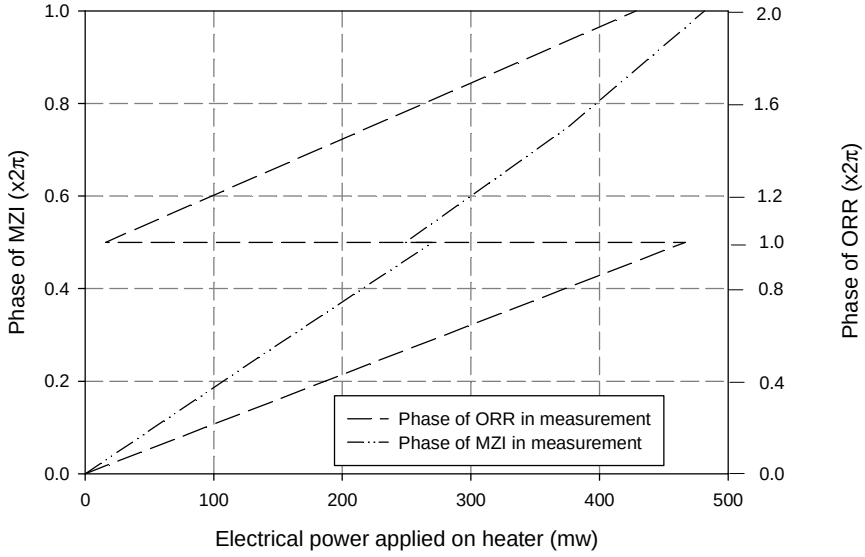

Figure 5.4 Phase and power relation in measurement

Figure 5.4 show the phase and power relation in the measurement. The phase of MZI should be a straight line, however there is a small offset when the phase is π, this is caused by the compensating the thermo crosstalk. The thermal crosstalk happens in between neighboring heaters on the chip. This kind of impact has been compensated by carefully choosing the voltage on heater in this measurement.

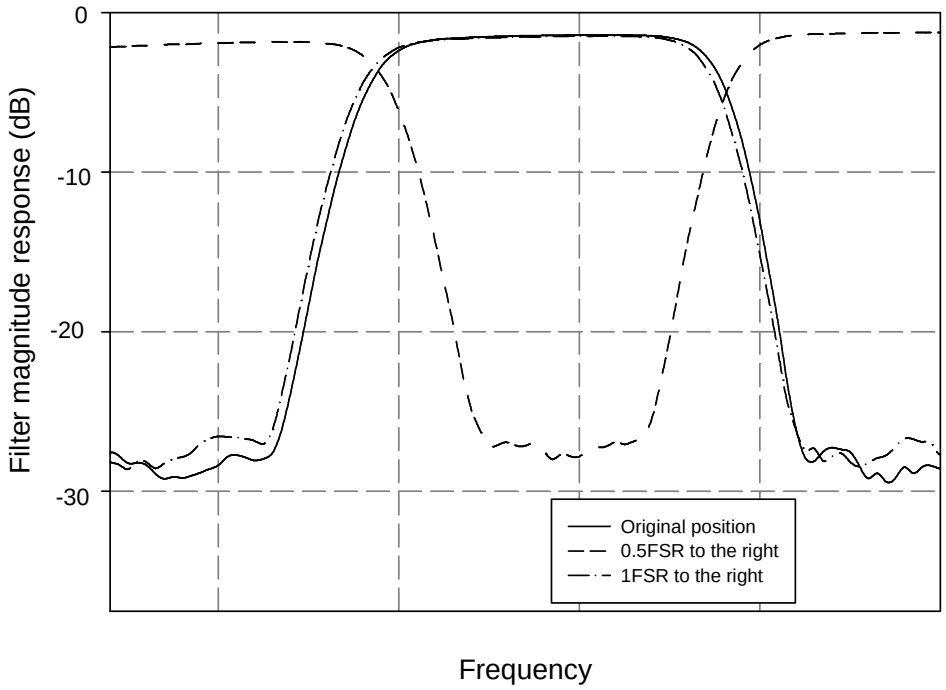

Figure 5.5: Filter response shifts for one FSR to the right

Figure 5.5 shows the measurement result for the filter response shifting. The filter shifting method shows good result, the center frequency of filter shifts to the right but the filter suppression remains the same, the stopband and passband bandwidth are not changed. This result shows that this filter have a tuning range of one entire FSR

5.2 Filter group delay response

The group delay response was measured for a MZI+ring filter with the FSR=6.7GHz. This measurement uses the same setup as previous one; but measured is the phase difference of the signal before and after passing the filter rather than the magnitude of the filter. This way

of measuring is known as the phase shift method [14]. The group delay is expressed in terms of phase as shown below:

$$\tau_g(\lambda) = \frac{\phi_{port2} - \phi_{port1}}{2\pi f_{cw}} \tag{5.2}$$

where ϕ_{port1} and ϕ_{port2} are the phase of the signal in port1 and port2 of the network analyzer. f_{cw} is the frequency of continuous wave signal, $f_{cw} = 100\text{MHz}$. It is not possible to measure the absolute group delay, since the total group delay is the sum of the delays of the extra fiber length, total length of the waveguides and the filter are unknown, but we are only interested in the variation of the delay, which comes from the filter.

The measurement result is shown in Figure 5.6. That is the group delay response within one FSR. The maximum and minimum group delay variation in the passband is 0.15ns. It has a good fitting to the data was achieved using the theoretical model of the filter. The fitted parameters of filter are $\kappa_1 = \kappa_2 = 0.5, \kappa_3 = 0.84$, Loss of ORR is1.9dB/cm.

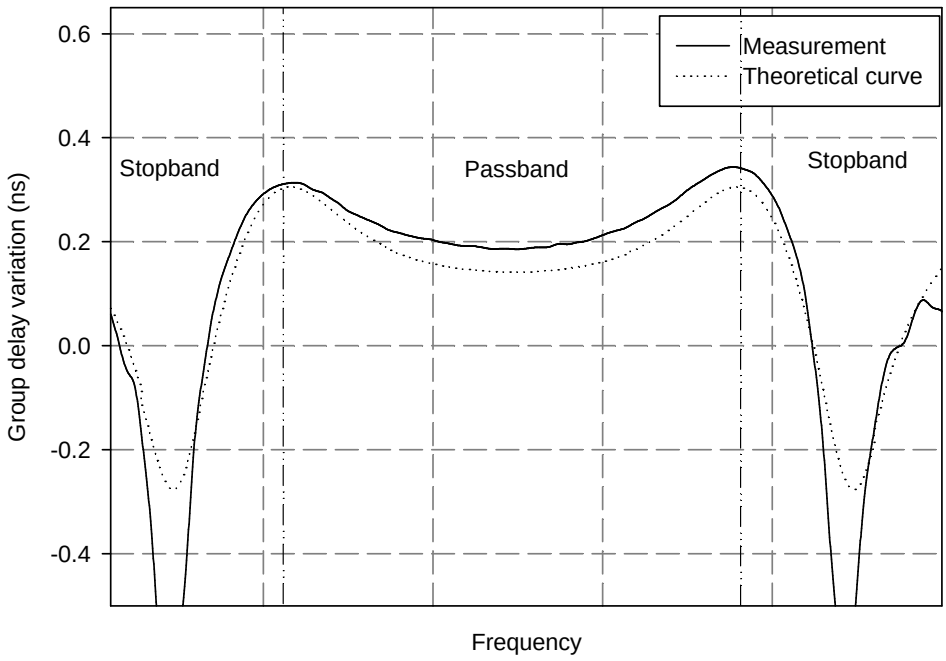

Figure 5.6: Group delay response of the filter

5.3 Single sideband suppressed carrier modulation

The implementation of optical SSB-SC signal has been explained in Chapter 2 in theory, in this section the experiment result is presented. The experiment setting is shown in Figure 5.7.

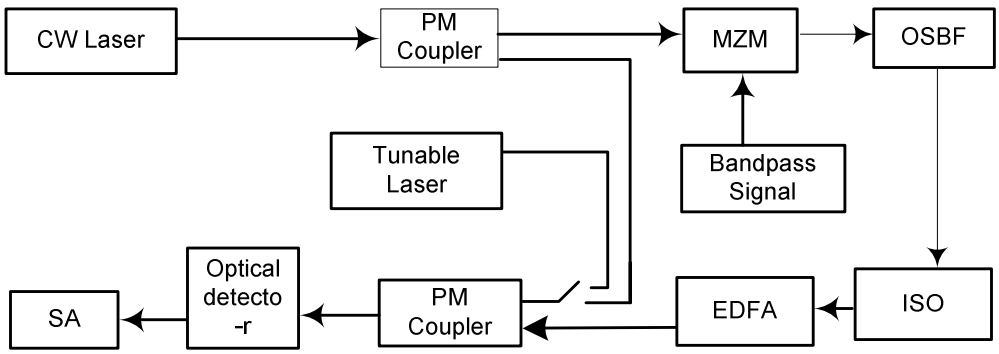

Figure 5.7: The setup for measuring SSB-SC signal

Continues wave laser with a wavelength of 1550.86nm is split by polarization maintaining coupler (PM coupler), PM coupler has been chosen for the case to maintain the interference of laser. The light has been spitted into two paths; one path is modulated with a bandpass signal. The other path is used to demodulate the SSB-SC signal. The original signal is a RF bandpass signal which has a bandwidth of 1GHz with the minimum frequency of 3GHz. We generated this signal by sweeping the frequency and holding the maximum value of the amplitude for each frequency. Then the modulated optical signal passes through the OSBF. The filter response is set to cut off one sideband together with the carrier. The SSB-SC signal is implemented. Isolator (ISO) is used for prevent the reflection from EDFA, which is used for optical signal amplification to overcome the signal attenuation from pervious stages. Carrier reinjection is done by PM coupler, together with optical detector, form a coherent detector. Then the RF signal is demodulated from optical carrier and visualized by spectrum analyzer (SA). In this measurement, the optical heterodyning technique is used before optical detection, in order to show the spectrum of SSB-SC signal..

The SSB-SC signal is shown in Figure 5.8.

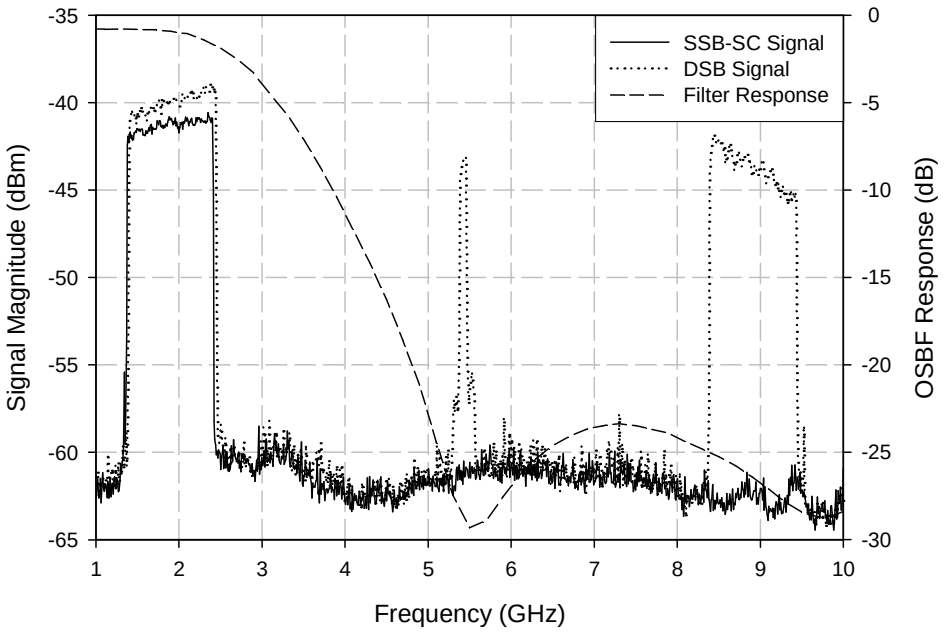

Figure 5.8: Filter based optical SSB-SC signal

The optical heterodyning technique shifts the spectrum of the modulated optical signal down into the frequency range of the RF spectrum analyzer. It is done by mixing the modulated light with Tunable laser. The peak between two sidebands indicates the frequency difference between the two heterodyning optical carriers. It shows that the magnitude of one sideband of the signal is 25dB suppressed

Chapter 6

6 Conclusions and recommendations

6.1 Conclusions

From the results obtained, if the date rate is increased, then the pulse is broadened more obvious, large overlapping may occur, it is dangerous for the two adjacent symbols with different signs, since the ISI caused by this overlapping would enlarge the BER at the receiver. One limiting factor of the filter is the data rate. This value is 2GS/s for the case the signal RF carrier is in the center of passband when the signal is modulated by QPSK modulation scheme. This value could be reduced to 1GS/s when the signal RF carrier is in the edge of the passband. The eye diagram for the DVB-S application is relatively clean for rectangle pulse. It indicates that there is very small ISI happened and the BER would not been changed due to this ISI. When RRC pulse is used, the ISI is zero. So this filter can be used with DVB-S signal.

This filter response can be optimized by five filter parameters, which correspond to five splitters/combiners and phase shifters. A tuning process in order to optimize filter response has been presented in this report. Thermal crosstalk exists between neighboring heaters in the measurement. This kind of crosstalk can be compensated by adjusting the voltage applied on heaters manually.

OSBF can be used to implement optical SSB-SC modulation. It is able to generate optical SSB-SC signal by suppressing one optical sideband of optical DSB-SC signal. For this purpose, a specified OSBF with a value of 25 dB stopband suppression is designed in [2]. In the measurement, this 25 dB suppression has been achieved. By using this optimized OSBF, the optical SSB-SC signal with 25dB suppression of one sideband has been implemented. This optical SSB-SC signal can be demodulated from optical domain to electrical domain by coherent detection.

.

6.2 Recommendations

Because of the thermal crosstalk between heaters, the accuracy of tuning is reduced. This thermal crosstalk is compensated manually in this research, however, it can also be compensate by some algorithms, then it could make the tuning more accurate.

The QPSK modulation is considered in this report; other modulation methods may need to be considered later on.

References

[1] A. Meijerink et al.,
"*Phase array antenna steering using a ring resonator-based optical beam forming network*"
13th IEEE/CVT Symposium Benelux, Liege, Belgium, 23 Nov. 2006, Paper 7-12

[2] Jorge Pena Hevilla
Optical sideband filtering in an optical beam forming system for phased array antennas
Master thesis, Chair of Telecommunication Engineering, Faculty of Electrical Engineering, Mathematics and Computer Science, University of Twente, Enschede, the Netherlands 2007

[3] Ulrich Reimers
Digital Video Broadcasting The International Standard for Digital Television 1st ed. Springer ,2001

[4] Roland Meijerink
Performance study of a ring resonator-based optical beam forming system for phase array received antenna,
Master thesis, Chair of Telecommunication Engineering, Faculty of Electrical Engineering, Mathematics and Computer Science, University of Twente, Enschede, The Netherlands 2007

[5] A. Nirmalathas, G.H. Smith, D. Novak,
"*Sensitivity analysis of optical SSB generation using a dual electrode Mach-Zehnder modulator*",
MWP 1998, New York, USA ,pp. 79-82, 12-14 Oct.1998.

[6] B. den Uyl,
Signal Sideband Modulation for optical beam forming in phased array antennas,
Bachelor thesis, Chair of Telecommunication Engineering, Faculty of Electrical Engineering, Mathematics and Computer Science, University of Twente, Enschede, The Netherlands 2006

[7] C.K. Madsen and J.H. Zhao,
Optical Filter Design and Analysis: A Signal Processing Approach,
John Wiley & Sons, Inc., New York, 1999

[8] Robert D.Strum and Donald E.Kirk
First Principles of Discrete Systems and Digital Signal Processing
Addison-Wesley Publishing Company, Inc. ,1988

[9] Simon Haykin,
Communication Systems, 3rd ed.
John Wiley & Sons, Inc., New York, 1994

[10] Simon Haykin, Michael Moher
Introduction to Analogy & Digital Communications 2nd ed.
John Wiley & Sons, Inc., New York, 2007

[11] ————
Squared Root Raised Cosine Filter
Institute of Communications Engineering
National Sun Yat-sen University, Taiwan, P.R.China
[Online] Available:
http://public.enst-bretagne.fr/~kouertan/BBIC-2-SRRC.pdf

[12] P.V.Lambeck, R.M.deRidder,
Optical Basic Functions and Microsystems
Study metrical, University of Twente, Enschede, The Netherlands,2005

[13] Chris Roeloffzen,
Passband flattened binary-tree structured add-drop multiplexers using SiON waveguide technology,
PhD dissertation (ISBN 90-365-1803-2), University of Twente, Enschede, The Netherlands, 2002

[14] K. Daikoku, A. Sugimura,
Direct measurement of wavelength dispersion in optical fibers-difference method,
Electron.Lett.,vol.14
pp.367,1978

Appendix A

Step response of filter

Here we show step response of filter in frequency domain. Since the MZI+ring filter is too complicated to be calculated and the principles of step response of filter are the same, we use a simpler filter expression to show the step response in frequency domain. Here we use MZI filter.

The step function in the time domain is expressed as :

$$u(t)=\begin{cases}1;\ t>0\\ 0;\ t<0\end{cases} \tag{A.1}$$

The Fourier transform of step function is:

$$U(\omega)=\pi\delta(\omega)+\frac{1}{\mathrm{j}\omega} \tag{A.2}$$

The frequency response of MZI is written as [7]:

$$H_{12}(\omega)=-\frac{\mathrm{j}}{2}\left[1+\exp(-\mathrm{j}\cdot\omega)\right] \tag{A.3}$$

The step response of this filter is given by:

$$\begin{aligned}Y(\omega)&=U(\omega)\cdot H_{12}(\omega)\\ &=\left[\pi\delta(\omega)+\frac{1}{\mathrm{j}\omega}\right]\cdot\left(-\frac{\mathrm{j}}{2}\left[1+\exp(-\mathrm{j}\cdot\omega)\right]\right)\end{aligned} \tag{A.4}$$

The inverse Fourier transform of (A.4)is:

$$y(t)=\frac{\mathrm{j}}{2}u(t)-\frac{\mathrm{j}}{2}u(t-1) \tag{A.5}$$

Equation (A.5) is a discrete time expression.

Both the time domain expression and frequency domain expression of the response of this MZI+ring filter show the discrete time behaviour.